Soil moisture and precipitation intensity jointly control the transit time distribution of quick flow in a flashy headwater catchment

Hatice Türk[1], Christine Stumpp[1], Markus Hrachowitz[2], Karsten Schulz[3] Peter Strauss[4], Günter Blöschl[5], and Michael Stockinger[1]

[1]University of Natural Resources and Life Sciences, Vienna, Department of Water, Atmosphere and Environment, Institute of Soil Physics and Rural Water Management, Muthgasse 18, 1190 Vienna, Austria
[2]Department of Water Management, Faculty of Civil Engineering and Geosciences, Delft University of Technology, Stevinweg 1, 2628CN Delft, the Netherlands
[3]University of Natural Resources and Life Sciences, Vienna, Department of Water, Atmosphere and Environment, Institute of Hydrology and Water Management, Muthgasse 18, 1190 Vienna, Austria
[4]Institute for Land and Water Management Research, Federal Agency for Water Management, Petzenkirchen, Austria
[5]Vienna University of Technology, Institute of Hydraulic Engineering and Water Resources Management, Karlsplatz 13, 1040 Vienna, Austria

Correspondence to: Hatice Türk, (hatice.tuerk@boku.ac.at)

Abstract. The rainfall-runoff transformation in catchments usually follows a variety of slower and faster flow paths, leading to a mixture of "younger" and "older" water in streamflow. Previous studies have investigated the time-variable distribution of water ages in streamflow (Transit Time Distribution, TTD) using stable isotopes of water ($\delta^{18}O$, $\delta^{2}H$) together with transport models based on StorAge Selection (SAS) functions. These functions are traditionally formulated based on soil moisture to mimic the preferential release of younger water as the system becomes wetter. In this study, we hypothesized that in a heterogeneous catchment with a significant fast runoff response component, precipitation intensity, in addition to soil moisture, plays a critical role in the preferential release of younger water. To test this hypothesis, we used high-resolution $\delta^{18}O$ data (weekly and event-based streamflow $\delta^{18}O$ samples) in a 66 ha agricultural catchment. We tested two scenarios of the SAS function parameterisation for the preferential flow age selection: one as a function of soil moisture only, and one as a function of both soil moisture and precipitation intensity. The results showed that accounting for both soil moisture and precipitation intensity to define the shape of SAS functions for preferential flow improved the tracer simulation in streamflow (increasing the Nash-Sutcliffe Efficiency from 0.31 to 0.51). This also led to a higher percentage of streamflow (an increase from 2.87% to 4.38%) with shorter transit times (TTs younger than 7 days) with the largest differences occurring during the summer and autumn months. This was due to the fact that incorporating both soil wetness and precipitation intensity in the SAS formulation accounts for rapid flow pathways such as infiltration-excess overland flow, preferential flow through macropores, and tile drain flow—allowing precipitation water to bypass much of the soil matrix and reach the stream with minimal storage or mixing, even under dry soil conditions. We showed for the agricultural study catchment that a significant portion of event water bypasses the soil matrix through fast flow paths), resulting in younger water reaching the stream for both low and high-intensity precipitation. Thus, in catchments where preferential flows and overland flow are dominant flow processes, soil-wetness-dependent and precipitation-intensity-conditional SAS functions may be required to better describe the time scale of solute transport in modelling, which has implications for stream water quality and agricultural management practices such as the timing of fertilizer application.

1 Introduction

The focus of hydrological research has expanded from the quantitative estimation of water fluxes to a better descriptions of underlying hydrological processes by estimating the water age of various storage and runoff components in catchments (Beven, 2006; McDonnell & Beven, 2014; Sprenger et al., 2019). Water age provides crucial information about the pathways through which water moves in catchments. This information can be used to quantify the time scale of the flow of precipitation through different pathways such as overland flow, lateral subsurface flow, and deep percolation. Such knowledge is useful for quantifying the fate of pollutants and sediments in catchments, which is essential for maintaining stream water quality and ensuring sustainable management of water resources.

The time it takes for precipitation to reach the stream is referred to as the water transit time, while water age is the time that has elapsed since precipitation entered the catchment (Rinaldo et al., 2011; Botter et al., 2011; Benettin et al., 2022).Depending on the physical characteristics of a catchment and on hydrometeorological conditions, transit times can vary from seconds to decades. Therefore, the knowledge of water transit time and its distribution (TTD) is essential for characterizing transport processes in catchments (McGuire & McDonnell, 2006; Botter et al., 2011; Klaus & McDonnell, 2013; Benettin et al., 2022). Despite their usefulness in studying water flow through catchments, TTs cannot be measured directly on a catchment scale, and they are instead inferred from catchment-wide input-output signals such as using the stable isotopes of oxygen ($\delta^{18}O$) and hydrogen ($\delta^{2}H$) in precipitation and streamflow (Kirchner et al., 2000; Fenicia et al., 2008; Fenicia et al., 2010; McGuire & McDonnell, 2006; Klaus & McDonnell, 2013; McDonnell & Beven, 2014; Benettin et al., 2022; Wang et al., 2025). $\delta^{18}O$ and $\delta^{2}H$ have been widely used to estimate the water transit times of precipitation parcels into different hydrological fluxes such as root water uptake, plant transpiration, lateral subsurface flow, and eventually streamflow (Hrachowitz et al., 2015; Abbott et al., 2016; Knighton et al., 2019; Knighton et al.,2020; Kübert et al., 2023).

Recent advances in sampling techniques now enable high-resolution stable isotope measurements, including hourly $\delta^{18}O$ of precipitation (von Freyberg et al., 2022; Welb et al., 2022) and sub-daily to daily $\delta^{18}O$ of streamflow (von Freyberg et al., 2022; Dahlke et al., 2014). Building on these data, several tracer-aided hydrological models have been developed to investigate the contributions of distinct runoff generation mechanisms by simultaneously solving water-, tracer-, and water-age balances (Botter et al., 2011), thereby providing estimates of water transit times (Hrachowitz et al., 2013; Benettin et al., 2015; Lutz et al., 2018; Kuppel et al., 2018; Remondi et al., 2019; Wang et al., 2023) as well as temporal variability in runoff generation processes (Kirchner et al., 2000; Fenicia et al., 2008; Fenicia et al., 2010; McGuire & McDonnell, 2006; Klaus & McDonnell, 2013; McDonnell & Beven, 2014; Benettin et al., 2022; Wang et al., 2025).

TTD estimation methods have recently evolved to describe the relationship between water storage and discharge in hydrological systems using the StorAge Selection (SAS) approach (Botter et al., 2011; Rinaldo et al., 2015). The SAS function characterizes the probability with which water parcels of different ages in a catchment's storage are released, thereby representing the relative contribution of young and old water to streamflow (Botter et al., 2011; Rinaldo et al., 2015). Since SAS functions cannot be directly observed, they are typically inferred from the calibration of a tracer-aided hydrological model that fits modelled tracer and streamflow signals to observed ones. They can be defined either as time-variable or time-invariable functions (Hrachowitz et al., 2013) with various functional shapes, such as beta (van der Velde et al., 2012), Dirac delta (Harman, 2015), or gamma (Harman, 2015) distributions.

Using SAS functions, previous studies have shown that TTDs are variable across time and space. Further, studies have shown the time-variability of SAS functions is controlled by soil moisture (soil storage), thus accounting for the higher probability of releasing a higher percentage of young water as a catchment's soils wet up (Harman, 2015; Hrachowitz et al., 2016; Benettin et al., 2017; Kaandorp et al., 2018; Harman, 2019). This is sometimes also referred toas the "inverse storage effect" (Harman, 2015). The wetness-dependent time-variability of SAS functions has been implemented in hydrological models to simulate tracer fluctuations in streamflow in catchments, such as Claduègne (Hachgenei et al., 2024), Gårdsjön (van der Velde et al., 2015), Elsbeek and Springendalse Beek (Kaandorp et al., 2018), Plynlimon (Benettin et al., 2015; Harman, 2015), and several Scottish catchments (Hrachowitz et al., 2013). This time-variable parameterisation of the SAS function depending on catchment wetness may be needed in catchments due to various factors. These factors include: (i) the dominance of a single process dependent on soil moisture conditions, like Hafren catchment in Wales (Benettin, et al., 2015; Harman, 2015), or saturation-excess overland flow in the Bruntland Burn catchment in Scotland (Benettin et al., 2017a); (ii) other site-specific hydrological characteristics that may be primarily influenced by catchment wetness.

Although preferential release of younger water is often accounted for in SAS functions through soil-moisture-dependent mechanisms, preferential release of younger water can also occur independently of the soil-moisture state when precipitation intensities exceed infiltration capacity. This is particularly critical for catchments where flow generation is not linearly related to soil storage, such as the flashy Weierbach catchment in Luxembourg (Rodriguez and Klaus, 2019), and for catchments where precipitation intensity and duration may play a critical role in how quickly water is mobilised from the landscape due to moderate to low soil infiltration capacity, such as the Hydrological Open-Air Laboratory in Austria (Vreugdenhil et al., 2022). Exclusively basing the shape of the SAS function on soil moisture may not fully capture the complexity of hydrological responses or all relevant transport processes, due to non-linear relationships between storage and streamflow (Danesh-Yazdi et al., 2018; Rodriguez & Klaus, 2019). Therefore, it remains to be tested whether accounting for precipitation intensity in addition to soil moisture to parameterize time-variable SAS functions may yield improved representations of stream tracer dynamics in specific environments.

The objective of this study is to test two alternative approaches to formulate the shape of time-variable SAS functions to account for the higher probability of releasing young water in a flashy headwater catchment: (i) exclusively soil moisture controls the SAS function shape for preferential release of younger water, and (ii) soil moisture and precipitation intensity jointly control the SAS function shape for preferential release of younger water. We hypothesize that in a heterogeneous catchment with a significant fast runoff response component, precipitation intensity, in addition to soil moisture, plays a critical role in the preferential release of younger water to the stream. To test this hypothesis, we used high-resolution δ18O data (weekly and event-based streamflow $\delta^{18}O$ samples) in the 66 ha agricultural catchment Petzenkirchen (Hydrological Open Air Laboratory, HOAL) in Austria. We addressed the following questions.

1. How does formulating the SAS function based solely on soil moisture reflect the streamflow tracer simulation and the inferred transit times?

2. How does formulating the SAS function based on soil moisture conditioned by precipitation intensity affect the streamflow tracer simulation in the catchment and the inferred transit times?

2 Methodology

2.1 Study Site

The Hydrological Open-Air Laboratory (HOAL) is a 66-hectare site located in Petzenkirchen, Austria (Fig. 1). The catchment is characterised by a humid climate with an average annual air temperature of 9.5°C. The mean annual precipitation and runoff are 823 mm yr^{-1} and 195 mm yr^{-1}, respectively. The year 2015 was notably dry (P = 580 mm yr^{-1}), while 2013, 2014, 2016, and 2017 had higher precipitation levels (> 700 mm yr^{-1}) and were classified as relatively wet years. The elevation ranges between 268 and 323 m above sea level, with an average terrain slope of 8%. The predominant soil types are Cambisols (57%), Planosols (21%), Kolluvisols (16%), and Gleysols (6%). The soils are characterized by a high clay content of 20–30% (Blöschl et al., 2016; Eder et al., 2014). Land use primarily includes agriculture (87%) (crop cultivation of maize, winter wheat, rapeseed, and barley), forest (6%), pasture (5%) and paved areas (2%) (Blöschl et al., 2016). Previous study in the catchment showed that the saturated hydraulic conductivity, Ks, exhibits substantial variability despite relatively limited spatial variation in physical and topographical soil properties. In arable fields, median Ks is approximately three times higher than in grassland areas, with arable land having a mean Ks of around 47 mm h^{-1} compared to 20 mm h^{-1} in grassland. Overall, Ks ranges over two orders of magnitude, from as low as 1 mm h^{-1} to as high as 130 mm h^{-1}, with a coefficient of variation (CV) of around 75 % in arable land (Picciafuoco et al., 2019). The concave part of the catchment (Fig. 1) was tile drained in the 1940s to reduce waterlogging because of the shallow, low-permeability soils and the catchment's use as agricultural land. The estimated drainage area from the tile-drains is about 15% of the total catchment area (Fig. 1).

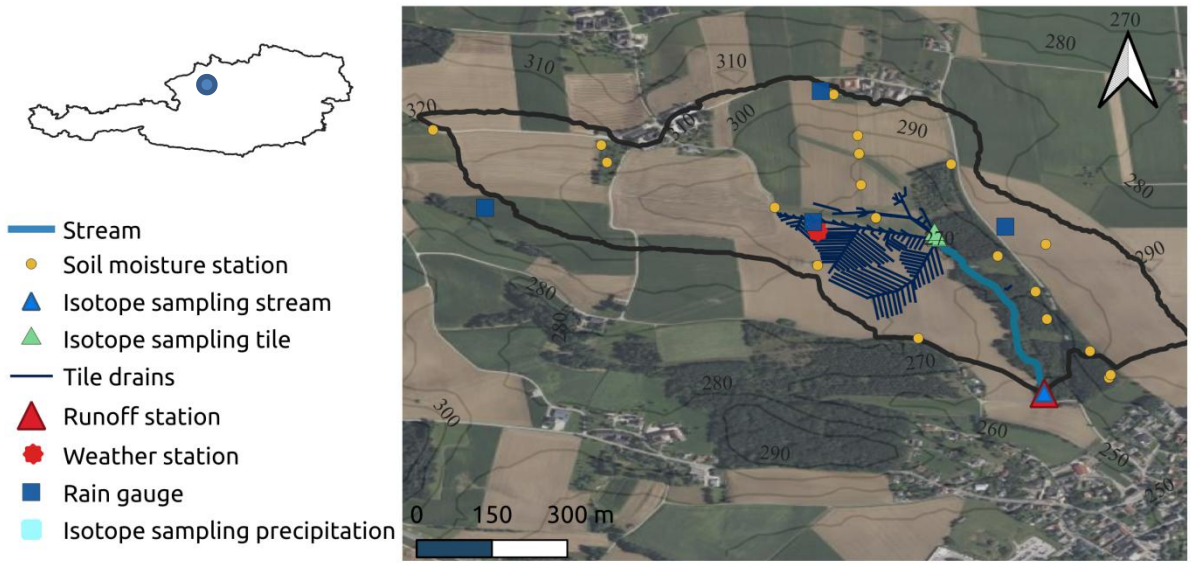

Figure 1. Map of the HOAL catchment (66 ha, Lower Austria) and location of rain gauges, a weather station, soil moisture stations, isotope sampling of streamwater, and isotope sampling of precipitation (located approximately 300 m south of the catchment, light blue circle) (map image from © Microsoft, Bing Maps via Virtual Earth)

2.1.1 Hydrometeorological data

Hydrometeorological data for the time period between October 2013 and December 2018 were used for the analyses (Fig 1. and Fig. 2a). Daily precipitation was available from four weighing rain gauges (OTT Pluvio). The arithmetic mean of the four rain gauges was used as the catchment average precipitation. Daily runoff at the catchment outlet was monitored using a

calibrated H-flume with a pressure transducer. Daily soil moisture in the unsaturated zone was available through 19 permanently-installed sensors. The catchment average soil water content was calculated across four different depths: 0.05 m, 0.10 m, 0.20 m, and 0.50 m. Sensor specifications and additional details about the hydrometeorological data are provided in Blöschl et al. (2016).

2.1.2 Stable isotope data

$\delta^{18}O$ measurements were available for the same period as the hydrometeorological data (Fig. 2b-d). Precipitation isotope samples (Fig. 2b) were collected using an adapted Manning S-4040 automatic sampler, located approximately 300 meters south of the catchment (Fig. 1). This sampler was coupled to a rain gauge and collected precipitation in 5 mm increments (corresponding to a 0.25 L sampling bottle). Once a bottle was filled, the sampler switched to the next bottle. Due to the limit of 5 mm per sample, it could happen that events with low rainfall amounts did not fully fill a sampling bottle, and the water from these events would then mix with water from the subsequent event or events in the same sampling bottle. For these events, the average concentration of temporally separated events was used. In addition to weekly grab samples (Fig. 2d), discharge water at the catchment outlet was collected during precipitation events using an Isco 6712 automatic sampler for the period from 2013 onwards (Fig. 2c). Similar to discharge, water samples were collected at the outlet of tile drains at two locations (Fig. 1) during precipitation events using an Isco 6712 automatic sampler. Sample collection for stream and tile drain water was based on specific flow rate thresholds, varying the sampling frequency from 15 minutes to 2 hours depending on the duration of the event (without exceeding sampling bottle capacity), an even distribution of sampling bottles was aimed for with adjusting the sampling frequency to the anticipated event duration. The analysis of these water samples for the stable isotopes of oxygen ($^{18}O/^{16}O$) and hydrogen ($^{2}H/^{1}H$) was done using Picarro L2130-i and L2140-i laser spectrometers (cavity ring-down spectroscopy). The measurement uncertainties were ±0.1‰ for $\delta^{18}O$ and ±1.0‰ for $\delta^{2}H$, respectively. All isotopic measurements are reported in per mil (‰) relative to Vienna Standard Mean Ocean Water (VSMOW). Both precipitation and streamflow event samples, as well as tile drainage samples, were aggregated to daily time intervals by calculating the volume-weighted average of the sampling fluxes based on their sampling frequency.

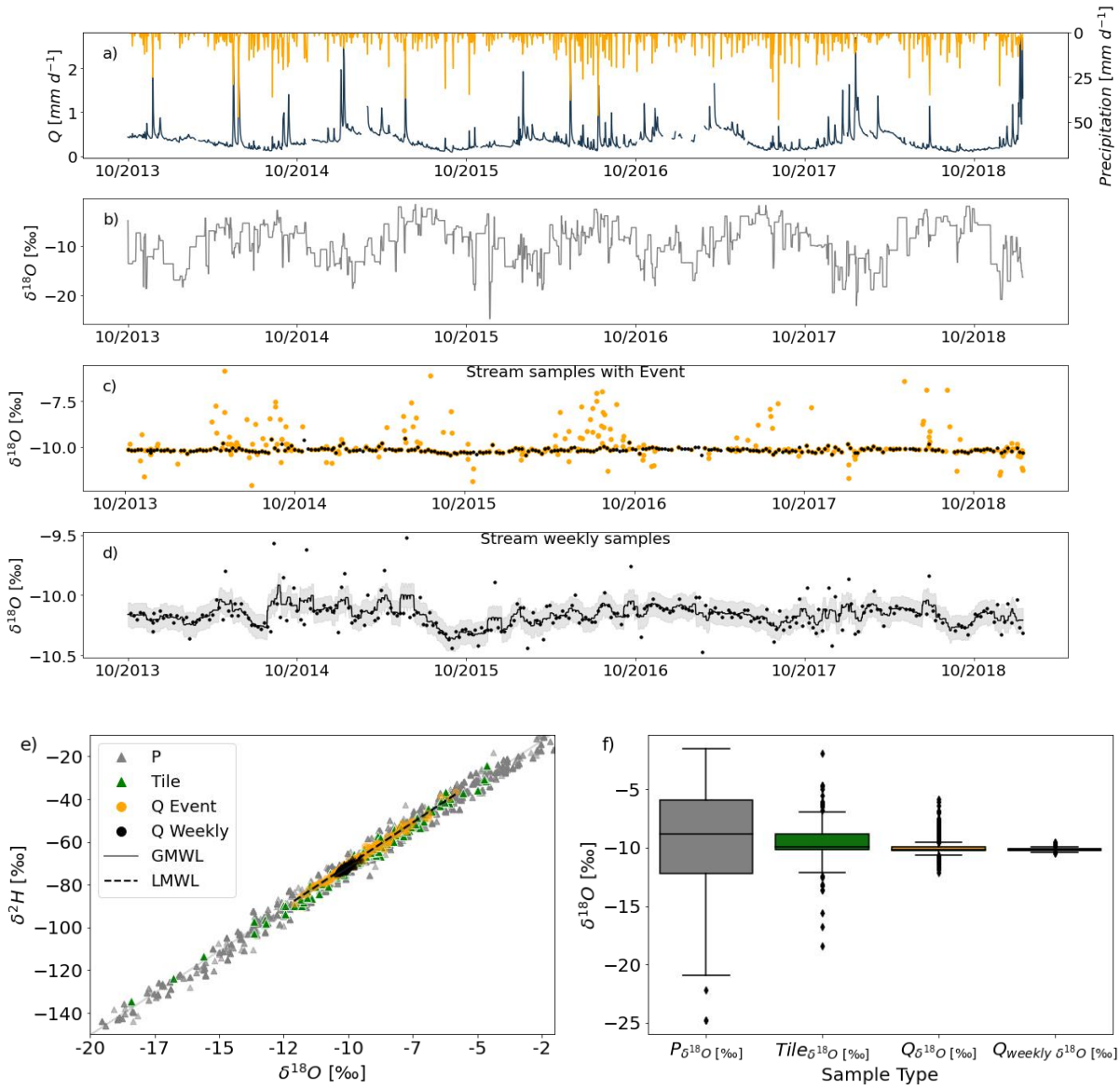

Figure 2. Hydrological and tracer data of the HOAL catchment (a) daily observed precipitation P (mm d^{-1}) and stream flow Q (mm d^{-1}) (b) $\delta^{18}O$ data from precipitation event samples at daily time scale (c) $\delta^{18}O$ data from streamflow with event (orange) and weekly grab samples (black) (d) weekly $\delta^{18}O$ data from streamflow where the gray shaded area shows the measurement uncertainty of ± 0.1‰ (e) dual plot of $\delta^{18}O$ and $\delta^{2}H$ from precipitation event samples (grey dots), streamflow event samples at daily time scale (orange dots), weekly grab samples (black) and tile drain event samples at daily time scale (green) (f) Box plot of $\delta^{18}O$ signal from precipitation event samples (gray box), tile drainage (green box), stream flow event (orange box) and weekly (black box).

2.2 Hydrological model structure

The process-based model used in this study consists of five reservoirs based on the previously developed DYNAMITE modeling framework (Hrachowitz et al., 2014; Fovet et al., 2015). The reservoirs represent the storage components for snow (S_{snow}, Eq. 1), canopy interception (S_i, Eq. 2), unsaturated root zone (S_r, Eq. 3), fast response (S_f, Eq. 4) and groundwater with active and passive components ($S_{S,a}$ and $S_{S,p}$, Eq. 5). Each of these had its own associated water fluxes (Fig. 3). The water balance and flux equations of the individual model components are given in Table 1 and a complete list of parameters and

their upper and lower bounds can be found in Table 2. A detailed model description and rationale for the assumptions in the model architecture can be found in previous studies (Hrachowitz et al., 2014; Fovet et al., 2015).

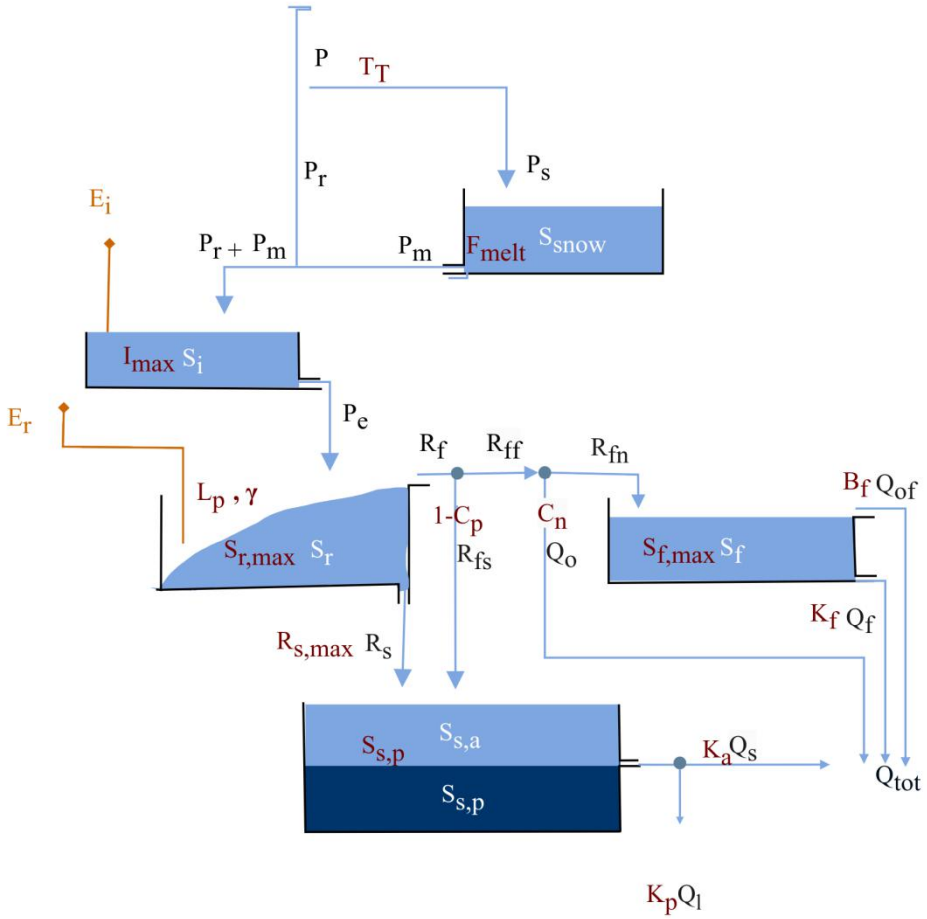

Figure 3. The model structure used to represent the HOAL catchment. Light blue boxes indicate the hydrologically active, individual storage volumes that contribute to total discharge (Q_{tot}): Snow storage (S_{snow}), canopy interception (S_i), fast-response bucket (S_f), root zone (S_r), and "active" groundwater ($S_{s,a}$). The darker blue box $S_{s,p}$ indicates a hydrologically "passive" mixing groundwater volume. Blue lines indicate snow and water fluxes while the orange lines indicate water vapour fluxes. Model parameters are shown in red adjacent to the model component they are associated with. All model equations are defined in Table 1, and symbols are defined in Table 2.

Table 1: Water balance and constitutive equations of the hydrological model (Fig.3). P (mm d^{-1}) is total precipitation, P_s (mm d^{-1}) is solid precipitation (snow), P_r (mm d^{-1}) is liquid precipitation (i.e., rain), P_m (mm d^{-1}) is snowmelt, P_e (mm d^{-1}) is throughfall, E_i (mm d^{-1}) is interception evaporation, E_a (mm d^{-1}) is evaporation from the root zone, R_f (mm d^{-1}) is total preferential fast response, R_{fs} (mm d^{-1}) is fast recharge to slow-responding reservoir, R_{ff} (mm d^{-1}) preferential fast response, Q_o (mm d^{-1}) is infiltration excess overland flow, R_{fn} (mm d^{-1}) is preferential fast response to the fast-responding bucket, Q_f (mm d^{-1}) is flow from the fast-responding reservoir, Q_{of} (mm d^{-1}) is saturation-excess overland flow from the fast-response bucket, R_s (mm d^{-1}) is slow recharge to the slow-responding reservoir, Q_s (mm d^{-1}) is flow from the slow-responding reservoir, Q_l (mm d^{-1}) is deep infiltration loss, and Q_{tot} (mm d^{-1}) is the total discharge. A list of model parameters and their definitions is provided in Table 2.

Storage Component and Water Balance	Eq.	Constitutive equations	Eq.
SnowBucket $\frac{dS_{snow}}{dt} = P_s - P_m$	(1)	$P_s = \begin{cases} P, & T < T_T \\ 0, & T \geq T_T \end{cases}$	(6)
		$P_m = \begin{cases} 0, & T < T_T \\ min(F_{melt}(T - T_T), \frac{S_{snow}}{dt}), & T \geq T_T \end{cases}$	(7)
Interception storage $\frac{dS_i}{dt} = P_r + P_m - P_e - E_i$	(2)	$P_r = \begin{cases} 0, & T < T_T \\ P, & T \geq T_T \end{cases}$	(8)
		$P_e = max(0, \frac{S_i - I_{max}}{dt})$	(9)
		$E_i = min(E_p, \frac{S_i - I_{max}}{dt})$	(10)
Soil storage $\frac{dS_r}{dt} = P_e - R_f - R_s - E_a$	(3)	$Cap = (1+\gamma)S_{r,max}\Big(1 - max(0, (1 - \frac{S_r}{S_{r,max}}))^{\frac{1}{1+\gamma}})\Big)$	(11)
		$R_f = P_e - S_{r,max} + S_r + S_{r,max}\Big(1 - \frac{(P_e + Cap)}{(1+\gamma)S_{r,max}}\Big)^{(1+\gamma)}$	(12)
		$R_s = min(R_{s,max}\frac{S_r}{S_{r,max}}, \frac{S_r}{dt})$	(13)
		$E_a = min\Big((E_p - E_i)min(\frac{S_r}{S_{r,max}L_p}, 1), \frac{S_r}{dt}\Big)$	(14)
Division fast recharge and fast flow and overland flow		$Rff = (C_p)R_f$	(15)
		$R_{fs} = (1 - Cp)R_f$	(16)
		$Q_o = \begin{cases} 0, & P_r < P_{tresh} \\ CnR_{ff}, & P_r \geq P_{tresh} \end{cases}$	(17)
		$Rfn = (1 - C_n)R_{ff}$	(18)
Fast responding Bucket $\frac{dS_f}{dt} = R_{fn} - Q_{of} - Q_f$	(4)	$Q_{Of} = max((S_f(\frac{S_f}{S_{f,max}})^{B_f} - S_{f,max}), 0)$	(19)
		$Q_f = max(0, (S_f(1 - \exp^{(-k_f t)})))$	(20)
Groundwater storage $\frac{dS_{s,a}}{dt} = R_s + R_{fs} - Q_s - Q_l$	(5)	$S_{s,tot} = S_{s,a} + S_{s,p} + R_s + R_{fs}$	(22)
		$Q_{s,tot} = \frac{S_{s,tot} - S_{s,tot,out}}{dt}$	(23)

$$\frac{Q_s}{Q_l} = max(0, \frac{k_a(S_{s,tot} - S_{s,p})}{k_p S_{S,tot}}) \quad (24)$$

$$Q_s = \frac{\frac{Q_s}{Q_l} Q_{s,tot}}{(\frac{Q_s}{Q_l} + 1)} \quad (25)$$

$$Q_l = \frac{Q_{s,tot}}{(\frac{Q_s}{Q_l} + 1)} \quad (26)$$

Table 2: Definitions and uniform prior distributions of the parameters of the solute-transport model (Fig. 3)

Parameter	Unit	Definition	Lower Bound, Upper Bound	Calibrated S1, S2
Hydrological				
T_T	(°C)	Threshold temperature for snow melt	[-4.0, 5.0]	[-2.90, -3.25]
γ	(–)	Shape factor	[0.0, 5.0]	[0.09, 0.19]
B_f	(–)	Saturation excess overland flow coefficient	[0.0, 0.00001]	[7.39e-6, 4.06e-06
C_n	(–)	Division parameter for fraction of overland flow	[0.0, 1.0]	[0.33, 0.18]
C_p	(–)	Division parameter for fast groundwater recharge	[0.0, 1.0]	[0.36, 0.28]
F_{melt}	(mmd^{-1} °C^{-1})	Melt factor	[1.0, 5.0]	[2.14, 1.65]
I_{max}	(mm)	Interception capacity	[1.2, 5.0]	[1.23, 1.82]
K_a	(d^{-1})	Storage coefficient of the slow-responding reservoir	[0.01, 1.2]	[0.19, 0.20]
K_f	(d^{-1})	Storage coefficient of the fast-responding reservoir	[0.01, 2.0]	[1.24, 0.85]
K_p	(d^{-1})	Storage coefficient of deep infiltration losses	[0.0, 0.00001]	[1e-05, 1e-04]
L_p	(–)	Transpiration water stress factor	[0.0, 1.0]	[0.55, 0.387]
P_{tresh}	(mm d^{-1})	Threshold precipitation for overland flow	[2.0, 20.0]	[9.92, 6.25]
$R_{s,max}$	(mm d^{-1})	Maximum percolation rate	[0.0, 1.2]	[0.61, 0.63]
$S_{f,max}$	(mm)	Fast response storage capacity	[0.0, 20.0]	[6.34, 4.25]
$S_{r,max}$	(mm)	Root-zone storage capacity	[100, 500]	[285, 382]
Tracer				**Tracer**
$S_{S,p}$	(mm)	Passive storage capacity	[1000, 10000]	[7555, 3173]
S_{U_Alpha}	(–)	SAS alpha shape parameter for root zone	[0.00, 1.0]	[0.03 0.06]
S_{G_Alpha}	(–)	SAS alpha shape parameter for GW	[0.98, 1.0]	[0.99, 0.99]

Precipitation P (mm d^{-1}) below the threshold temperature T_T (°C) enters the catchment as snow P_s (mm d^{-1}, Eq. 6) and accumulates in the snow bucket S_{snow} (mm). Snowmelt P_m (mm d^{-1}) was then computed with the degree-day method (Eq. 7), driven by the melt factor F_{melt} (mm d^{-1} $°C^{-1}$) as described by Gao et al. (2017) and Girons Lopez et al. (2020). Rainwater P_r (mm d^{-1}), combined with snow melt P_m (mm d^{-1}) passes through the canopy interception storage S_i (mm). Water that is not evaporated as interception evaporation E_i (mm d^{-1}, Eq. 10) enters the unsaturated root zone S_r (mm) as throughfall P_e (mm d^{-1}, Eq. 9) based on the water balance of the canopy interception storage (Nijzink et al., 2016) (Eq. 2). Water from the root zone S_r (mm) can either be released as (i) fast discharge R_f (mm d^{-1}, Eq. 12), which is based on a critical storage capacity, Cap, calculated using $S_{r,max}$ and the shape factor γ (-) (ii) slow recharge to the active groundwater storage $S_{s,a}$ (mm) through a slower percolation flux R_s (mm d^{-1}, Eq. 13) which is driven by the maximum percolation rate $R_{s,max}$ (mm d^{-1}) (iii) the combined flux of root-zone transpiration and soil evaporation E_a (mm d^{-1}, Eq. 14) defined by the transpiration water stress factor L_p (–). The fast, preferential discharge R_f (mm d^{-1}) is subsequently divided in several steps to account for fast flow paths. These are the preferential flow recharging groundwater R_{fs} (mm d^{-1}, Eq. 15), the infiltration-excess overland flow reaching streamflow Q_o (mm d^{-1}, Eq. 16) which is regularly observed in the HOAL catchment (Blöschl et al., 2016) and the lateral subsurface flux R_{fn} (mm d^{-1}, Eq. 17). Firstly, the fast groundwater recharge R_{fs} (mm d^{-1}, Eq. 15) is defined by the division parameter (1-C_p). The remaining water R_{ff} (mm d^{-1}, Eq. 15) is then further divided to account for infiltration-excess overland flow Q_o (mm d^{-1}, Eq. 16) which is defined by the division parameter C_n *(-)* and the threshold parameter P_{tresh} (mm d^{-1}) (Horton, 1933). We assumed a constant value for the division parameter C_n (-) to limit the number of calibration parameters in the spirit of model parsimony. After subtraction of fast groundwater recharge and overland flow, the remaining fast and lateral subsurface flux R_{fn} (mm d^{-1}, Eq. 17) enters the fast storage component S_f (mm, Eq. 4). If the maximum capacity of S_f (mm, Eq. 4) is exceeded, water was released as saturation excess overland flow Q_{of} (mm d^{-1}, Eq. 18). Otherwise, it was released to the stream as fast flow Q_f (mm d^{-1}, Eq. 19).

Groundwater storage was separated into an "active" groundwater storage $S_{s,a}$ and a hydrologically "passive" storage volume $S_{s,p}$ (mm). $S_{s,p}$ (mm) does not change over time if there are no deep infiltration losses, so that $dS_{S,p}/dt=0$ (Zuber, 1986; Hrachowitz et al., 2016; Wang et al., 2023). This "passive" storage does not contribute to runoff but its role is to isotopically mix water of the "active" storage with water of the "passive" storage which is represented as $S_{s,tot} = S_{s,a} + S_{s,p}$. The use of the total groundwater storage $S_{s,tot}$ facilitates contributions from both $S_{s,a}$ and $S_{s,p}$ to the age structure of the outflow Q_s (mm d^{-1}, Eq. 24). Water enters the groundwater storage as a sum of slow percolation R_s (mm d^{-1}) and fast recharge R_{fs} and is released as base flow Q_s (mm d^{-1}, Eq. 24) and deep infiltration losses Q_l (mm d^{-1}, Eq. 25).

2.3 Tracer transport model

2.3.1 Rank StorAge Selection (rSAS) function

We combined the hydrological model, as described in the previous section, with a transport model that utilizes the age-rank StorAge Selection (rSAS) function which ranks stored water volumes by age (Harman, 2015; Benettin et al., 2017) to capture the variability of outflow ages over time. The general theoretical framework of the transport model relies on the studies of Botter et al. (2009), van der Velde et al. (2012), Harman (2015), and Benettin et al. (2015). At any given time, t, each storage $S_{T,m,j}(t)$ defined within the hydrological model (Fig. 2) stores water of different ages. These ages are represented as T and trace back to past precipitation inputs at age $T = 0$. The age distribution of storage at time t is termed $p_s\ (T,t)$. The outfluxes (e.g., evapotranspiration and discharge) consist of specific age subsets from the storage, resulting in distinct age-ranked distributions for the water leaving the storage. These are termed $p_{E,T}\ (T,t)$ for evapotranspiration and $p_{Q,T}(T,t)$ for

discharge. At each given time t, the total water volume in storage is also characterized by its tracer composition and distributions $C_S(T,t)$ which traces back to past precipitation inputs. In the case of an ideal tracer, it is equal to the water stable isotope composition of past precipitation ($P_{\delta}{}^{18}O$) upon entering the catchment at time t-T, i.e., $C_P(t-T)$. As a result, output fluxes are characterized by water stable isotope compositions ($Q_{\delta}{}^{18}O$, $Q_{\delta}{}^{2}H$) and $C_Q(t-T)$ for streamflow, and ($ET_{\delta}{}^{18}O$, $ET_{\delta}{}^{2}H$) and $C_{ET}(t-T)$ for evapotranspiration.

2.3.2 Integration of the rSAS function concept and the hydrological model

The water age balance (Equation 27) was formulated individually for each of the j storage components of the model such as canopy interception or the root zone, based on their transport dynamics. The change in water storage is the difference between age-ranked input volumes $I_{T,j}(T, t)$ (mm d^{-1}) and age-ranked output volumes $O_{T,j}(T, t)$ (mm d^{-1}) (Botter et al., 2011; Harman, 2015; and van der Velde et al., 2012).

$$\frac{\delta S_{T,j}(T,t)}{\delta t} + \frac{\delta S_{T,j}(T,t)}{\delta T} = \sum_{n=1}^{N} I_{T,n,j}(T,t) - \sum_{m=1}^{M} O_{T,m,j}(T,t) \tag{27}$$

$\partial S_{T,j}(T,t)/\partial T$ is the aging process of water in storage, N and M are the number of inflows and outflows from that storage component (e.g., for the root zone these would be E_a, R_f, and R_s (Fig. 3). Each age-ranked outflow $O_{T,m,j}(T, t)$ (Equation 28) from a specific storage component j (Fig. 3) depends on the outflow volume $O_{m,j}(t)$ which was estimated by the hydrological balance component of the model (see section 2.2) and the cumulative age distribution $P_{o,m,j}(T, t)$ of that outflow.

$$O_{T,m,j}(T,t) = O_{m,j}(t) P_{O,m,j}(T,t) \tag{28}$$

The cumulative age distribution $P_{o,m,j}(T, t)$ (Eq. 29), which is the backward transit time distribution TTD of that outflow in cumulative form, depends on the age-ranked distribution of water in the storage component j, represented by $S_{T,j}(T, t)$ for time step t and the probability density function, which in this case is SAS function $\omega_{o,m,j}$ (or $\Omega_{o,m,j}$ in its cumulative form) of that flux.

$$P_{O,m,j}(T,t) = \Omega_{O,m,j}(S_{T,j}(T,t),t) \tag{29}$$

The SAS function $\omega_{o,m,j}$ (or $\Omega_{o,m,j}$ in its cumulative form) is a probability density function of normalized rank storage $S_{T,norm,j}(T,t)$ (Eq. 31) at time t, which can also be formulated as the residence time distribution RTD of storage component j (e.g., root zone) at time t (Eq. 30). Normalizing the age-ranked storage prevents rescaling of $\omega_{o,m,j}$ at each time step to conserve mass balance. Therefore, we used normalized rank storage (Eq. 5) to bind the age-ranked storage to the interval [0,1].

$$p_{O,m,j}(T,t) = \overline{\omega}_{O,m,j}(S_{T,j}(T,t),t)\frac{\delta S_{T,j}}{\delta T} \tag{30}$$

$$S_{T,norm,j}(T,t) = \frac{S_{T,j}(T,t)}{S_j(t)} \tag{31}$$

The $\delta^{18}O$ composition from entering the catchment as precipitation to leaving it as streamflow were tracked through each individual storage component based on the tracer balance (Eq. 32) (e.g., Harman, 2015; Benettin et al., 2017).

$$C_{O,m,j}(t) = \int_0^{S_j} C_{S,j}(S_{T,j}(T,t))\omega_{O,m,j}(S_{T,j}(T,t),t)dS_T. \quad (32)$$

Where $C_{o,m,j}$ is the $\delta^{18}O$ composition in outflow m from storage component *j* at time *t*, and $C_{s,j}$ is the $\delta^{18}O$ composition of water in storage at time *t*.

2.3.3 Time-variable and conditional SAS functions

Previous studies found a difference in transport processes between wet and dry periods (Weiler and McDonnell, 2007; Beven, 2010; Beven and Germann, 2013; Klaus et al., 2013; Loritz et al., 2017; Hrachowitz et al., 2021; Wang et al., 2025). This suggests that SAS functions are time-variable and can be formulated as varying between preferential release of younger water, preferential release of older water, or no preference (uniformly selected) (van der Velde et al., 2012; van der Velde et al., 2015; Hrachowitz et al., 2016).

In this study, we used beta distributions with shape and scale parameters $\alpha(-)$ and $\beta(-)$ as SAS functions. When both parameters of the beta distributions are equal to 1 ($\alpha = \beta = 1$), water was uniformly sampled from storage without a preference for specific ages. If $\alpha < \beta$ (or $\alpha > \beta$), a selection preference for younger (or older) water existed. To limit the number of parameters, we kept "β" equal to 1. The time variability of the SAS function shape was then based on age-ranked storage and the shape parameter (α), which was bounded between [0,1] for the preference of younger storage and was [α>1] for the preference of older storage. In the following, we used this approach for the root zone storage S_r. In contrast, all other storage components (e.g., snow, groundwater) were based on uniform sampling ($\alpha = 1, \beta = 1$). Despite the shape parameters being fixed to uniform sampling in each of these storage components, the resulting overall SAS function, aggregating the individual storage components, was nevertheless time-variable due to the different time scales of, and the temporally-varying contributions, from the individual components (Eq. 30).

Previous studies have shown that as soil moisture increases, preferential flow increasingly bypasses small pore volumes, leading to the release of younger water (Weiler and McDonnell, 2007; Beven, 2010; Loritz et al., 2017; Hrachowitz et al., 2021). To mimic this behaviour, SAS functions for the fast preferential flow R_f (mm d^{-1}) were formulated with a time-variable shape factor $\alpha(t)$ (Fig. 4), which varied between 0 and 1 for each time step *t*. The variation of α(t) was implemented by following Hrachowitz et al. (2013) and van der Velde et al. (2015), by varying it as a function of the stored water volume $S_r(t)$ and the maximum storage capacity ($S_{r,max}$), as shown in Equation 33 and Figure 4 (Scenario 1):

$$\alpha(t) = 1 - \frac{S_r(t)}{S_{r,max}}(1 - \alpha_0) \quad (33)$$

where α_0 is a calibration parameter representing a lower bound between [0,1], so that $\alpha(t)$ can vary between α_0 and 1; $\alpha(t) = 1$ indicates a uniform sampling SAS function at low soil moisture (dry soil) (Fig. 4a, A). This formulation (Scenario 1, Fig. 4a) leads to an increasing preferential release of younger water as the system becomes wetter.

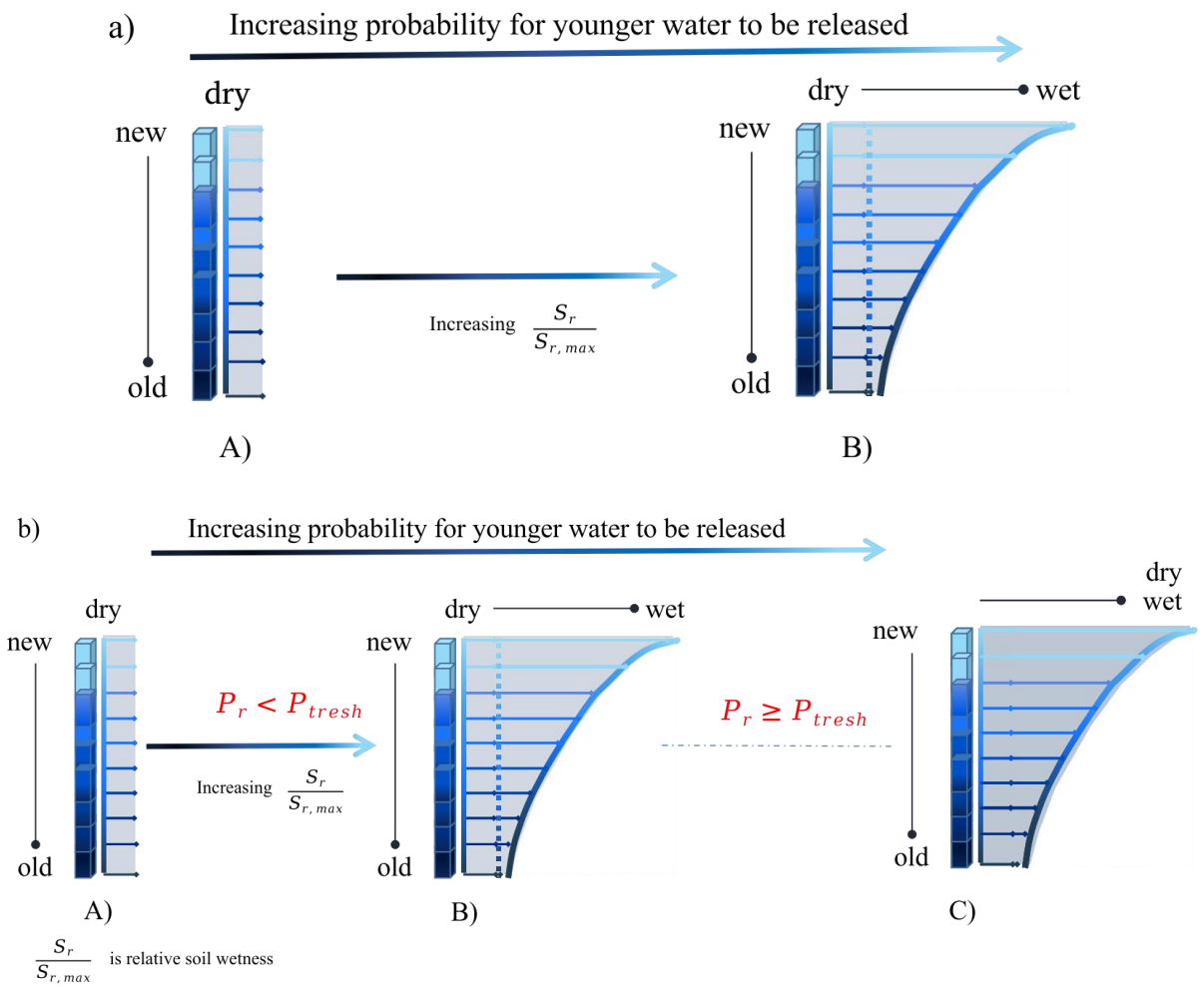

295 **Figure 4.** The two tested scenarios for determining the shape of the time-variable SAS function for the fast flux R_f (mm d^{-1}) (Fig. 3). The age-ranked storage probability function is shown as vertical bars in all panels (A, B, and C), with the light blue colour representing young water (at the top of the vertical bars), while the dark blue colour represents old water (at the bottom of the vertical bars). (a) In scenario 1 (S1), -the time-variable SAS function depends on the ratio of the current storage S_r to the maximum storage capacity $S_{r,max}$, with the preference for young water increasing as storage increases from A to B (Eq. 33). (b) In scenario 2 300 (S2), -the condition (A to B) only applies when the precipitation intensity does not exceed the threshold intensity (P_{tresh}). If it does exceed P_{tresh}, young water is preferentially released from storage (panel C), regardless of the current wetness state. This mimics rainfall bypassing the soil storage as fast overland or subsurface lateral flow.

Previous research highlighted the non-linearity of flow processes in the HOAL catchment, where precipitation can quickly generate fast runoff and bypass the soil storage as fast overland or subsurface lateral flow (Blöschl et al., 2016; Exner-305 Kittridge et al., 2016; Vreugdenhil et al., 2022; Hövel et al., 2023; Szeles et al., 2024). To mimic and test this in our study, SAS functions for the fast preferential flow, R_f (mm d^{-1}), were formulated with a time-variable shape factor, $\alpha\ (t)$, which varies as a function of soil moisture, as it is in Equation 33 (Scenario 1, Fig. 4a), but additionally became equal to α_0 (-) (lower bound) when precipitation intensity P_I (mm d^{-1}) exceed a certain threshold P_{tresh} (Scenario 2, Fig. 4b, Eq. 34) .

$$\alpha(t) = \begin{cases} \alpha_0, & \text{if } P_r(t) \geq P_{tresh} \\ 1 - \frac{S_r(t)}{S_{r,max}}(1-\alpha_0), & \text{if } P_r(t) < P_{tresh} \end{cases} \quad (34)$$

This formulation (Scenario 2, Fig. 4) leads to (i) an increasing preferential release of younger water with increasing soil moisture, and (ii) a higher probability of releasing younger water that bypasses the soil-stored water when precipitation intensity P_I (mm d^{-1}) exceed the threshold intensity (P_{tresh}).

2.4 Model optimization

The model was run with a daily time step for the time period between October 2013 and 30 December 2018 to calibrate the 15 hydrological and 2 tracer transport model parameters (Table 2). We used the one year data from October 2013 to October 2014 as warm-up period. Using an objective function that combines six performance criteria (Table 3) related to streamflow and tracer dynamics, we implemented the Differential Evolution algorithm (Storn and Price, 1997) to optimise model parameters.

For model calibration and evaluation, we used six performance metrics (Table 3) that describe the model's ability to simultaneously reproduce different signatures associated with streamflow Q (mm d^{-1}), and $\delta^{18}O$ dynamics of the streamflow (Eq. 35). These are the Nash-Sutcliffe Efficiencies (NSE) (Nash and Sutcliffe, 1970) of streamflow, of the logarithmic streamflow, of the flow duration curve, and of the time series of seasonal runoff ratios (averaged over three months). For $\delta^{18}O$ signals, we used the NSE of $\delta^{18}O$ of all measured samples (daily event and weekly grab samples) (Fig. 2c) and the mean square error (MSE) of weekly grab samples (Fig. 2d). Similar to Wang et al. (2024), the individual performance metrics were aggregated into the Euclidean Distance, D_E, to the perfect model, using equal weights for the six stream flow and two tracer signatures, respectively, according to:

$$D_E = \sqrt{\frac{1}{2}\left(\frac{\sum_{i=m}^{M}(1-E_{Q,m})^2}{M} + \frac{\sum_{i=n}^{N}(1-E_{18O,n})^2}{N}\right)} \tag{35}$$

where M is the number of performance metrics with respect to streamflow, N is the number of performance metrics for tracers in each combination, and E is the evaluation matrix based on goodness-of-fit criteria. D_E is the Euclidean distance to the 'perfect model', with zero indicating a perfect fit. We selected the 50 best parameter sets ranked by decreasing Euclidean distance, D_E, for model evaluation.

We used two scenarios for model calibration, where the formulation for hydrological fluxes was identical, but the transport formulation differed for the lower bound of the SAS function shape, α_0 (-), as described in Section 2.3.3: Scenario 1 (S1), -with $\alpha(t)$ being a linear function of wetness ($S_r/S_{r,max}$) (Eq. 33), and Scenario 2 (S2), -with $\alpha(t)$ being a linear function of wetness ($S_r/S_{r,max}$) if precipitation intensity was less than the threshold intensity, P_{tresh}. However, if precipitation intensity exceeded the threshold intensity (P_{tresh}), $\alpha(t)$ was set to a strong preference for young water release, with shape factor $\alpha(t) = \alpha_0$ (-) (Eq. 34).

2.5 Model comparison and data analysis

We evaluated the performance of the model under two scenarios using six performance metrics, which are listed in Table 3, for the tracking period from October 2014 to December 2018. Next, we analyzed transit times in relation to hydrological and hydroclimatic drivers by categorizing water into different age thresholds. These thresholds included: $T < 2$ days and $T < 7$ days, representing "event" water; $7 < T < 90$ days, representing young water with some delay; and $90 < T < 365$ days,

representing longer transit times. The streamflow age fraction F_Q ($T < T_{age}$ days) was calculated based on the sum of TTD, where $T < T_{age}$ days. For example, the age fraction of streamflow, F_Q ($T < 90$ days), was calculated based on the sum of TTDs, where $T < 90$ days.

We calculated the mean and maximum percentage of streamflow fractions for transit times $T < 2$ days, $T < 7$ days, $T < 90$ days, $7 < T < 90$ days, and $90 < T < 365$ days. We also compared the variation in mean and maximum percentage of streamflow water age fractions for different seasons: autumn (September, October, November), winter (December, January, February), spring (March, April, May), and summer (June, July, August), as well as for distinct wetness states (dry, drying, wet, and wetting periods). Dry days were marked by flows less than the 25th-quantile, while wet days were marked by flows higher than the 75th-quantile. Drying days marked any decay between the 25th-quartile and 75th-quartile whereas wetting days were marked as any increase between the 25th-quartile and 75th-quartile.

Furthermore, we compared the relationship between transit times and hydrological and hydroclimatic drivers, specifically, streamflow Q (mm d^{-1}), precipitation intensity P_I (mm d^{-1}), and volumetric soil water content SWC (%) for the tracking period, as well as across different seasons and wetness states, to understand variations in the control mechanisms. This analysis was conducted by comparing Spearman rank correlation coefficients of water age fractions with the hydroclimatic drivers.

Table 3: Signatures for streamflow, the $\delta^{18}O$ signal, and the associated performance metrics used for model calibration scenarios and evaluation.

Signatures	Abbreviation	Performance Metric	Reference
Time series of streamflow	Q	NSE_Q $NSE_{(logQ)}$	Nash and Sutcliffe (1970)
Flow duration curve	FDC	NSE_{FDC}	Jothityangkoon et al. (2001)
Seasonal runoff ratio	RC	NSE_{RC}	Yadav et al. (2007)
Times series $\delta^{18}O$ in streamflow	$\delta^{18}O$	$NSE_{\delta^{18}O}$ $MSE_{\delta^{18}O}$	Birkel et al. (2011a)

3 Results

3.1 Model calibration

The model parameters selected for the HOAL catchment during the calibration period from October 2014 to December 2018 reproduced the general features of the hydrograph (Fig. 5). The best-performing model generally captured both the timing and magnitude of high and low flow events, independent of the selected scenario ($NSE_Q = 0.61$ for both scenarios, Fig. 5a), with the exception of overestimations of low flows during summer 2016 and underestimation of low flows during winter

2017. The three-month averaged runoff ratio (RC) was reproduced, with NSE values of 0.89 for Scenario 1 and 0.83 for Scenario 2 (Fig. 5b, e). The flow duration curve (FDC) was also reproduced, with a Nash-Sutcliffe efficiency (NSE_{FDC}) of 0.51 for Scenario 1 and 0.50 for Scenario 2 (Fig. 5d,e). Additionally, low flows were reproduced, with a median Nash-Sutcliffe efficiency of log-flows (NSE_{logQ}) of 0.65 (Fig. 5c,e). For several rain storms, the model reproduced the sharp $\delta^{18}O$ fluctuations during events and a highly stable $\delta^{18}O$ signal between consecutive events (Fig. 5c) for both scenarios. However, Scenario 2 indeed showed considerable improvements for the very negative winter $\delta^{18}O$ stream values in 2015 and 2018, as well as for several events in summer 2016, 2017, and 2018. The performance metrics based on median $\delta^{18}O$ signals were higher for Scenario 2. with e.g., an $NSE_{\delta^{18}O} = 0.51$, than for Scenario 1, with an $NSE_{\delta^{18}O} = 0.31$ (Fig. 5e). Overall, the Euclidian distance D_E for the 50 best performing parameter sets decreased from 0.55 to 0.42 for Scenario 1 and decreased from 0.57 to 0.37 for Scenario 2, showing that Scenario 2 performed generally better than Scenario 1. For both scenarios, the MSE for weekly samples ($MSE_{\delta^{18}O}$) were comparable (Fig. 5e).

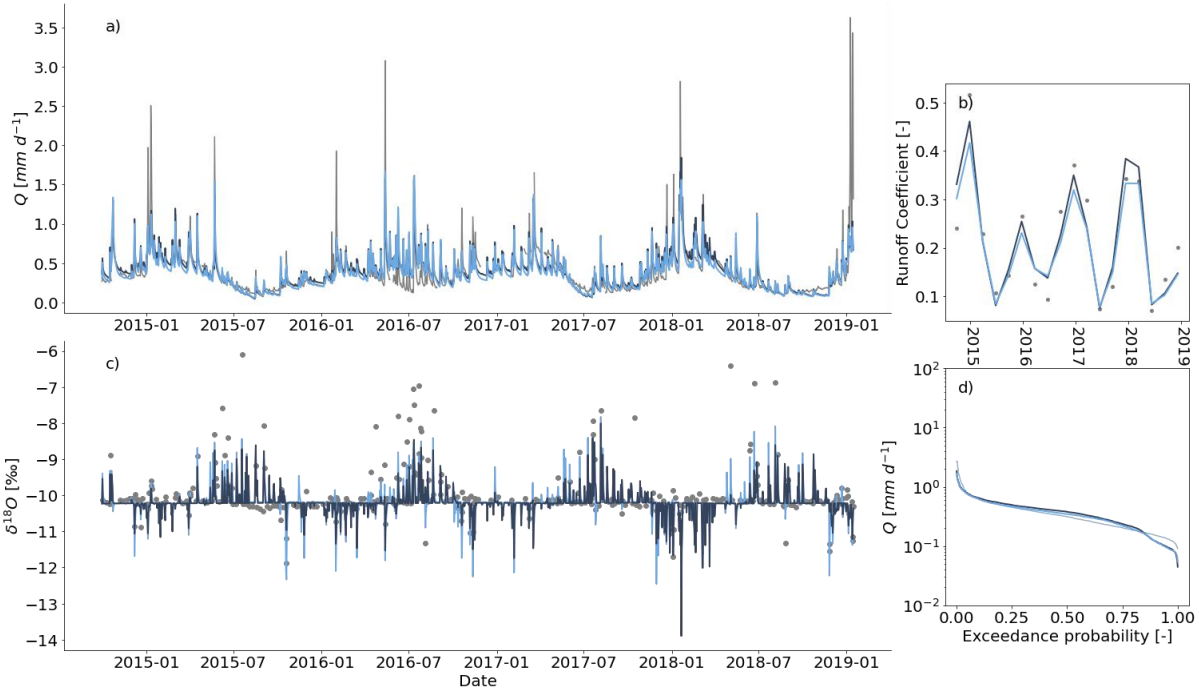

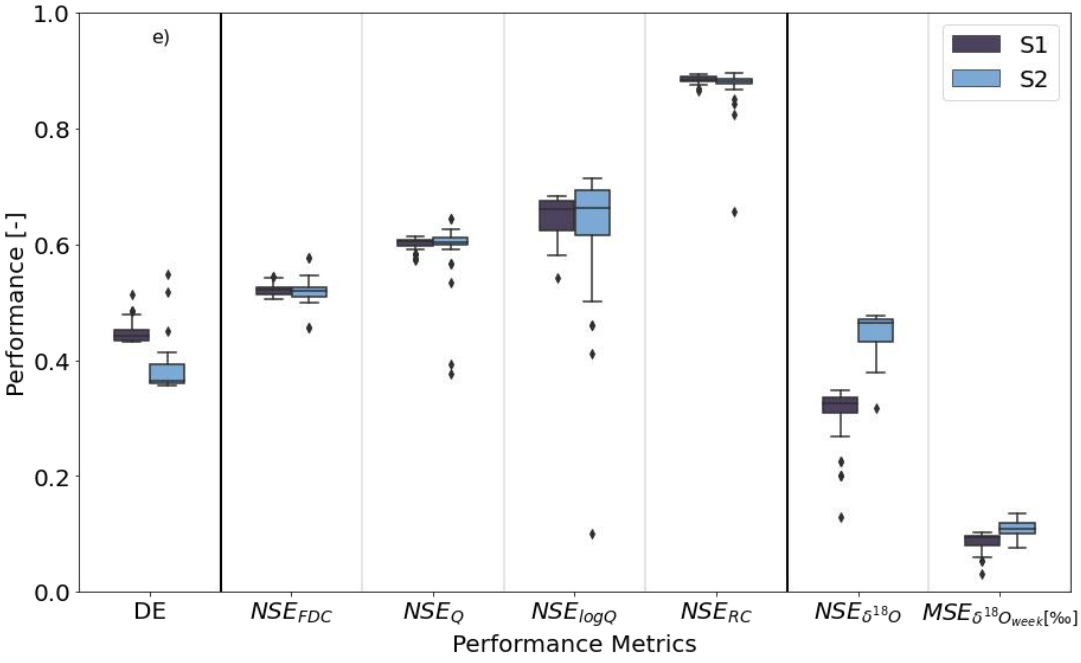

380

Figure 5. Model calibration results for Scenario 1 (S1, dark blue) and Scenario 2 (S2, light blue) (a, d) where the observed values are shown as gray dots and lines. (a) streamflow [mm d^{-1}], (b) streamflow ^{18}O [‰], (c) the three-month average runoff coefficient *RC* [-], (d) the flow duration curve [mm d^{-1}], and (e) boxplots of performance metrics of the two scenarios based on the 50 best performing parameter sets.

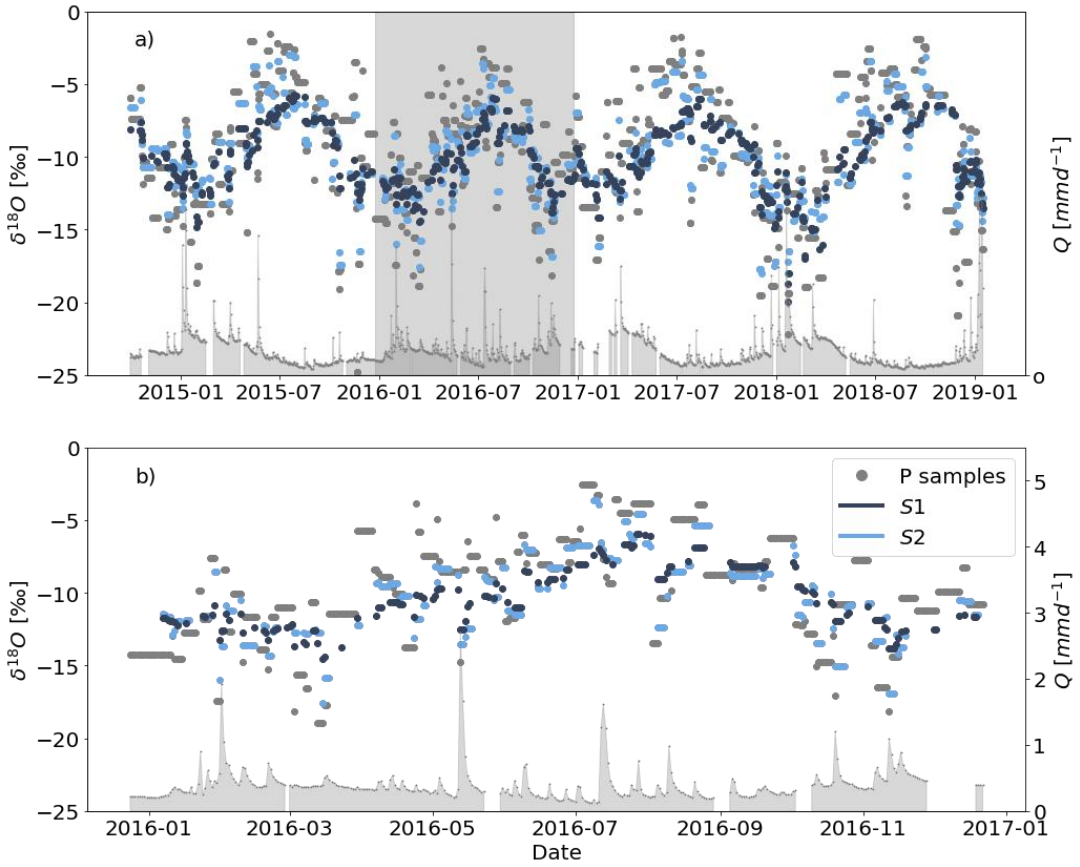

385

Figure 6: $\delta^{18}O$ simulations of preferential flow under two scenarios: Scenario 1 (S1, dark blue dots), where the SAS function was based solely on soil moisture, and Scenario 2 (S2, light blue dots), where it additionally accounted for precipitation intensity. In S1, the $\delta^{18}O$ signal was more dampened, indicating a larger contribution of old water to preferential flow. In contrast, S2's $\delta^{18}O$

response more closely aligned with the precipitation input, reflecting a more direct contribution of event water to streamflow. (b) zoom-in to the $\delta^{18}O$ simulations of preferential flow under two scenarios for the year 2016.

Simulated $\delta^{18}O$ from preferential flow (*RF*) is shown in Figure 6. In Scenario 1, where the SAS function for preferential flow is exclusively controlled by soil moisture, the simulated $\delta^{18}O$ signal in stream water was noticeably more dampened compared to Scenario 2. This reflects a higher probability of mobilising older stored water, reducing the direct transmission of event water to the stream. In contrast, Scenario 2, which incorporated both soil moisture and precipitation intensity, resulted in a modelled stream water $\delta^{18}O$ signal that more closely resembled both, the observed stream water $\delta^{18}O$ as well as the precipitation input signal. This highlights that accounting for precipitation intensity allows the model to better capture dynamic preferential flow responses, with a higher probability of mobilising younger event water into the stream.

3.2 Water transit times and residence times

By tracking the $\delta^{18}O$ signals through the model, we estimated TTDs in streamflow and compared these distributions for different age thresholds, namely $T < 2$ days, $T < 7$ days, $7 < T < 90$ days, $T < 90$ days, and $90 < T < 365$ days (see Section 2.4). It is important to acknowledge that the transit time results are inherently tied to the assumptions made and the uncertainties within the modelling process.

Model calibration based on Scenario 2 resulted in more younger water bypassing storage as evidenced by the mean percentage of streamflow age fraction younger than 2 days F_Q ($T < 2$ days) and 7 days F_Q ($T < 7$ days) being lower for Scenario 1 (2, 27% and 2.87%, respectively) compared to Scenario 2 (3.78 % and 4.03 %) (see Table 4, Fig. 7a and Fig. S2). This was also reflected in individual TTDs for fast preferential flow R_f (mm d^{-1}) (Fig. 3), where on average 40 % of fast preferential flow was from recent rainfall (age = 1 day) based on S2 compared to 30% for S1 (Fig. 7e). However, the fraction of streamflow that is younger than 90 days, F_Q (T < 90 days), was similar for both scenarios where the mean percentage for Scenario 1 was 6.03 % and for Scenario2 it was 6.53 % (see Table 4 and Fig. 7b).

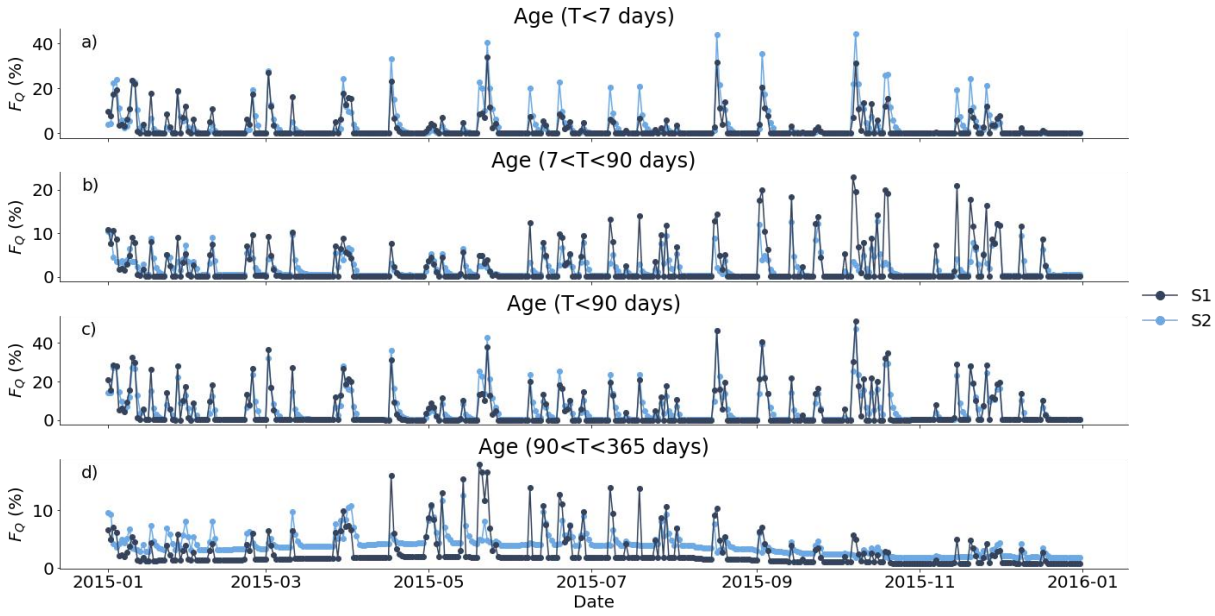

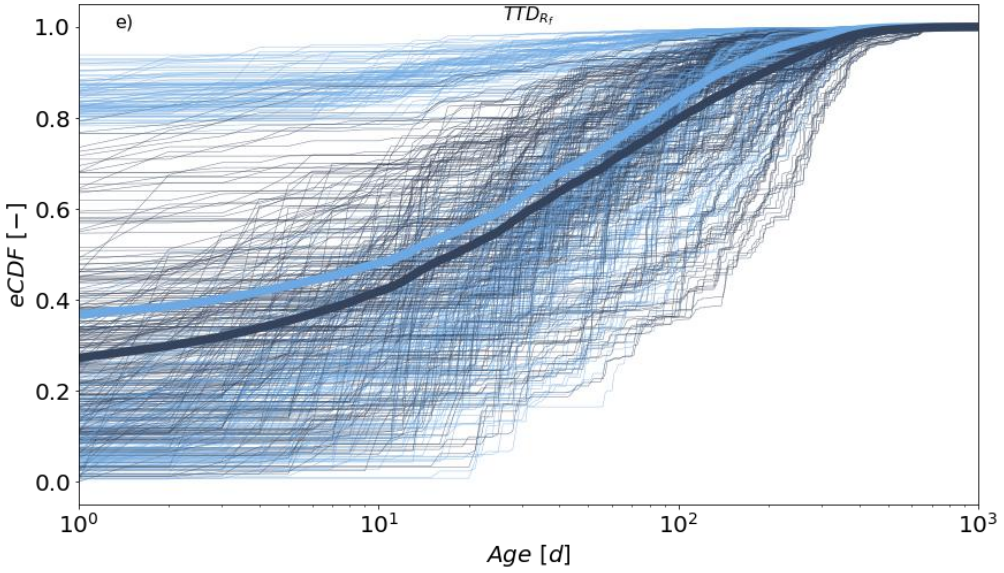

Figure 7. The percentage of water age fractions based on two scenarios for the year 2015 (a-d). The results for the full calibration period are provided in Supplementary Figure S2. In panels (a-e), dark blue dots represent the results from Scenario 1 (S1), and light blue dots represent the results from Scenario 2 (S2). The age fraction of streamflow was categorized by age: (a) $T < 7$ days, (b) $7 < T < 90$ days, (c) $T < 90$ days, and (d) $90 < T < 365$ days. Panel (e) shows individual transit time distributions (TTD) based on Scenario 1 and Scenario 2 for total fast preferential flow R_f (Fig. 3) as empirical cumulative distribution functions, eCDF(-). The bold lines in panel (e) show the mean of individual TTDs in cumulative form based on Scenario 1 (dark blue line) and Scenario 2 (light blue line).

Table 4: Summary of the mean and maximum (max) percentage of water transit times (categorised by $T < 90$, $0 < T < 2$, $0 < T < 7$, $7 < T < 90$, $90 < T < 365$ in days) based on Scenario 1 and Scenario 2.

Transit time (day)	S1		S2	
	mean (%)	max (%)	mean (%)	max (%)
$T < 90$	6.03	52.99	6.53	48.47
$0 < T < 2$	2.27	35.37	3.78	45.80
$0 < T < 7$	2.87	36.41	4.38	45.89
$7 < T < 90$	2.83	25.73	2.15	14.46
$90 < T < 365$	2.67	24.90	3.59	17.27

3.3 Influence of hydrological and hydroclimatic variables on water age fractions

The influence of hydrological and hydroclimatic variables on water age fractions ($0 < T < 7$, $T < 90$, $90 < T < 365$ in days) was compared by Spearman rank correlation coefficients (r, p). Only the precipitation intensity P_I (mm d^{-1}) was strongly correlated with the streamflow water age fraction younger than 7 days, F_Q ($T < 7$days), for both scenarios, with a slightly higher correlation coefficient for Scenario 1 (S1, $r = 0.67$, $p < 0.05$) compared to Scenario 2 (S2, $r = 0.53$, $p < 0.05$) (Fig. 8b). Similarly, water age fractions younger than 90 days, F_Q ($T < 90$ days), were more correlated with precipitation intensity P_I (mm d^{-1}) than with volumetric soil water content SWC (%), or streamflow Q (mm d^{-1}) (Fig. 8d, 8e, 8f). The correlation coefficients (r and p) with P_I (mm d^{-1}) were $r = 0.71$ and $p < 0.05$ for Scenario 1, and were $r = 0.62$ and $p < 0.05$ for Scenario 2.

For streamflow age fractions between 90 and 365 days, $F_Q(90 < T < 365$ days), only Scenario1 resulted in strong correlation coefficients with P_I (mm d^{-1}) (r = 0.58, p < 0.05) (Fig. 8h). No strong correlations were found for all other combinations of the water age fractions to Q (mm d^{-1}) or SWC (%) (Fig. 8).

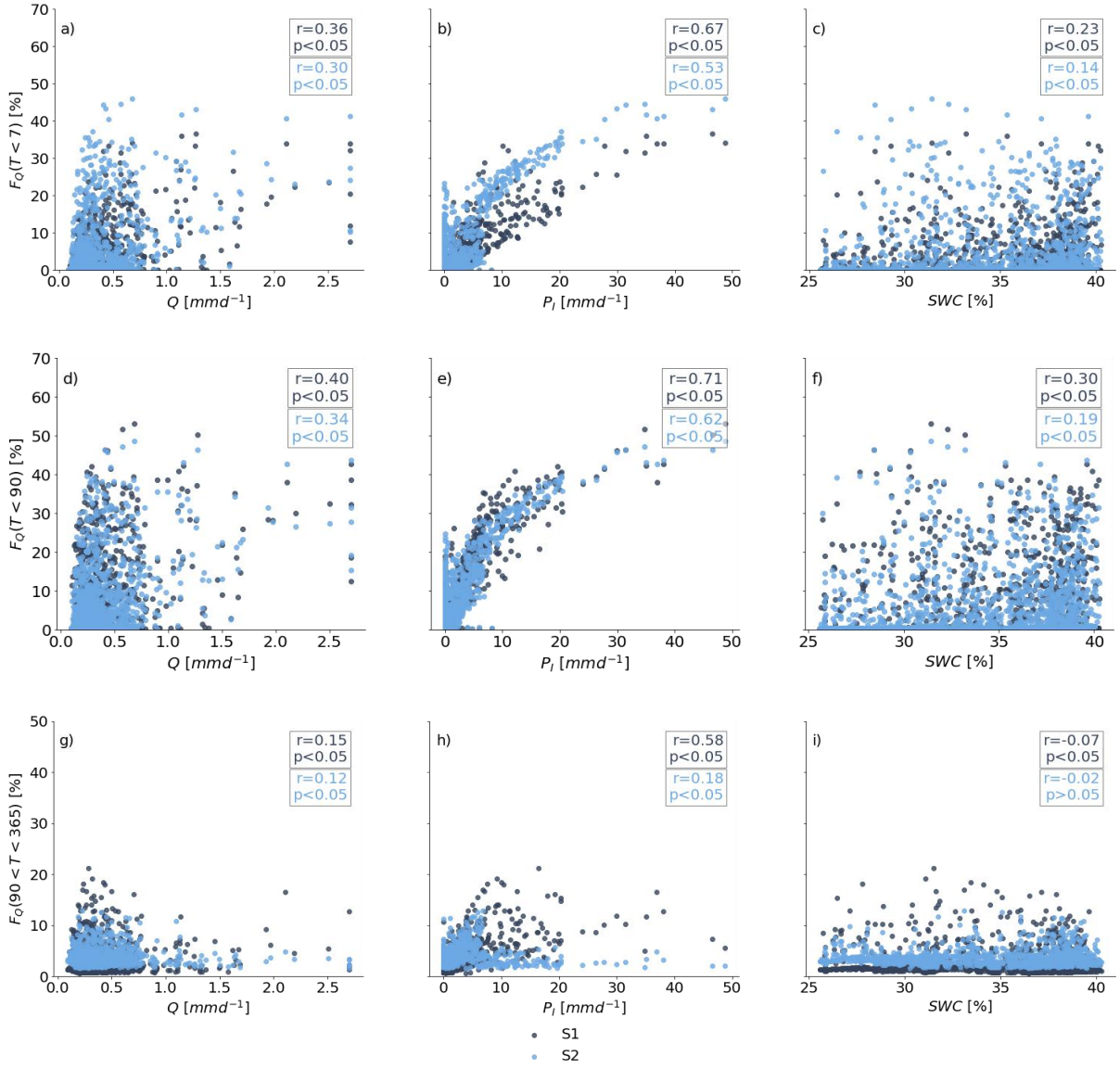

Figure 8. Spearman rank correlation of streamflow water age fractions with the hydrological and hydroclimatic variables, discharge Q [mm d^{-1}], precipitation intensity P_I [mm d^{-1}], and volumetric soil water content SWC [%]. Panel (a, b, c) show the correlations of streamflow age fractions younger than 7 days $F_Q(T < 7$days), (d, e, f) show the correlations of streamflow age fractions younger than 90 days $F_Q(T < 90$ days) and (g, h, i) correlations of streamflow age fractions older than 90 days but younger than 365 days $F_Q(90 < T < 365$ days) to discharge Q [mm d^{-1}], precipitation intensity P_I [mm d^{-1}], and volumetric water content SWC [%] respectively.

3.4 Linking water age fractions to hydrological and hydroclimatic drivers in different seasons

Scenario 2 resulted in a higher fraction of streamflow water younger than 7 days $F_Q(T < 7$days), especially during autumn and summer, compared to Scenario 1 (Fig. 9a, 10a). However, during spring and winter, both scenarios reproduced similar results for $F_Q(T < 7$days). On average, 2 % and 4 % of autumn streamflow was younger than 7 days based on Scenario 1 and Scenario 2, respectively. For individual events, these values reached up to a maximum of 31 % and 44 % based on Scenario 1 and Scenario 2, respectively (Table 5). Similarly, in the summer season, Scenario 2 resulted in a higher fraction of streamflow younger than 7 days, with an average of 4.48% compared to Scenario 1 (3 %). For water ages $7 < T < 90$ days

and 90 < T < 365 days, Scenario 1 resulted in higher streamflow fractions across all seasons compared to Scenario 2 (Fig. 10b, 10c; Table 5)

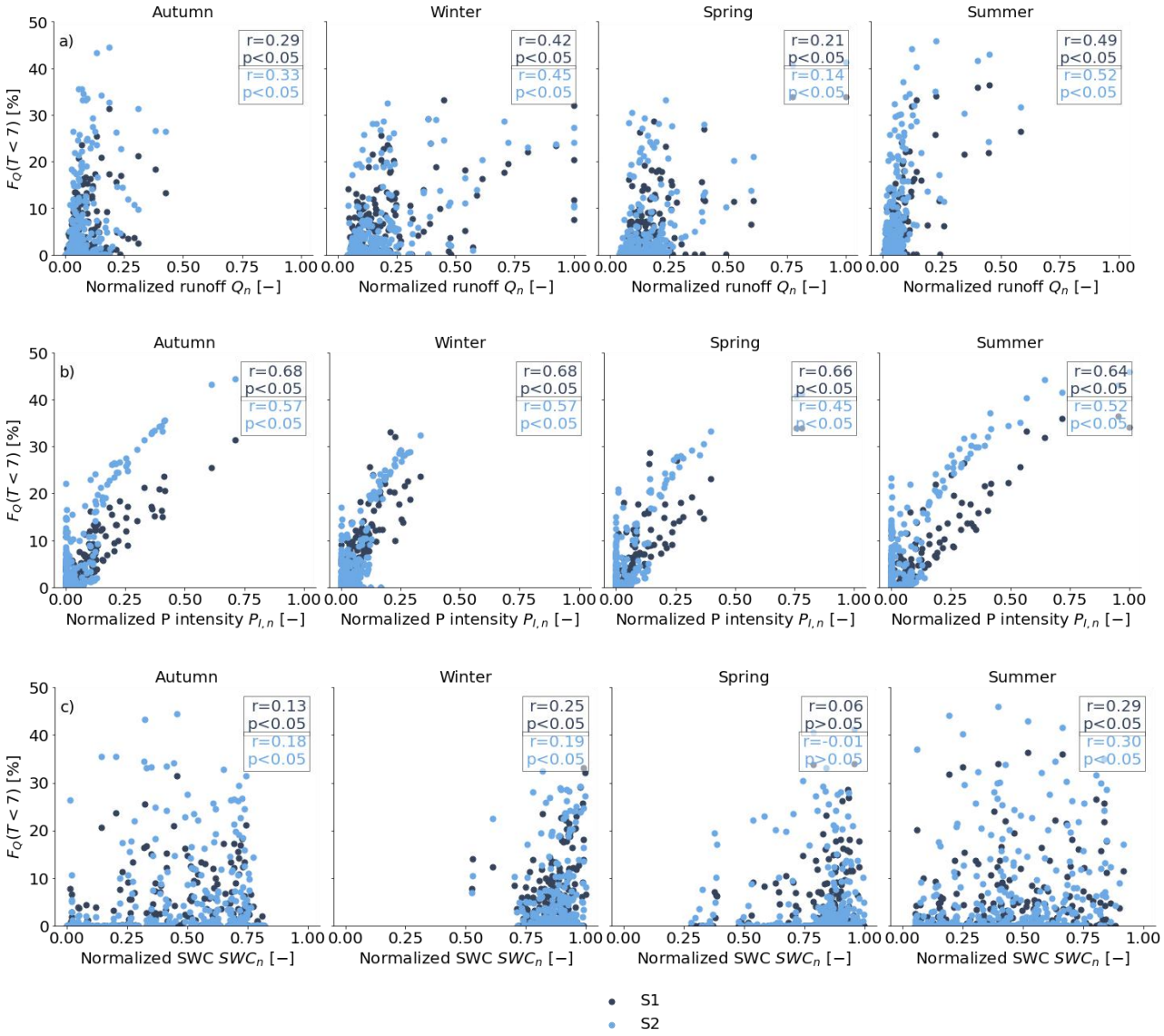

Figure 9. Spearman rank correlation of streamflow water age fractions younger than F_Q (T < 7 days) with hydrological and hydroclimatic variables across different seasons (autumn, winter, spring, summer). (a) Normalised discharge, Q [-], correlated with F_Q (T < 7 days), (b) normalised precipitation intensity, $P_{I,n}$ [-], correlated with F_Q (T < 7 days), (c), and normalised volumetric water content, SWC [-], correlated with F_Q (T < 7 days).

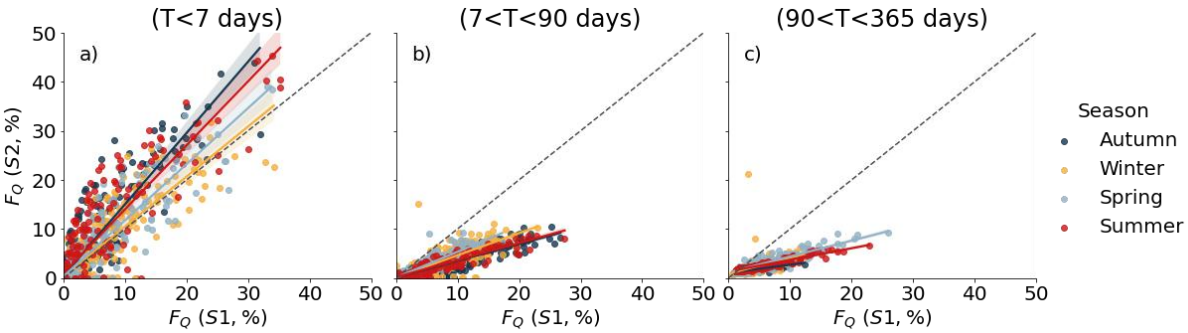

Figure 10: Comparison of estimated water ages based on two scenarios. Streamflow age fraction results from Scenario 1 are represented on the x-axis, while results from Scenario 2 are represented on the y-axis. The black dashed lines represent the 1:1 line for all panels. The comparison of estimated water age fractions younger than 7 days (a), age fractions from 7 to 90 days (b), and age fractions between 90 to 365 days (c) are shown. The colours indicate different seasons (dark blue: autumn, yellow: winter, light blue: spring, and red: summer)

Table 5: Summary of the mean and maximum (max) percentage of water transit times (categorised by age $0 < T < 7$, $7 < T < 90$, $90 < T <$ 365 in days) based on Scenario 1 and Scenario 2 for autumn, winter, spring, and summer.

		S1				S2			
Transit time (day)		Autumn	Winter	Spring	Summer	Autumn	Winter	Spring	Summer
$0 < T < 7$	mean(%)	2	4	3	3	4	4	4	5
	max (%)	31	33	34	36	44	32	41	46
$7 < T < 90$	mean(%)	3	3	2	3	2	3	2	2
	max (%)	26	20	15	24	14	13	10	13
$90 < T < 365$	mean(%)	2	2	3	3	3	4	4	4
	max (%)	12	11	25	21	7	17	15	13

4 Discussion

4.1 Soil moisture is not the only control of transit times

Previous studies have shown that soil moisture plays a significant role in catchment transit times in humid areas, such as the Wüstebach in Germany and the Bruntland Burn catchment in Scotland (Benettin et al., 2017; Hrachowitz et al., 2021). However, in the HOAL catchment of this study, rainfall intensity, beyond soil moisture, was required to account for the complexity of the hydrological and transport response.

For both scenarios (S1: SAS function with soil moisture only, S2: SAS function with soil moisture and rainfall intensity), the mean fraction of relatively short travel times in stream water ($T < 7$, $7 < T < 90$, and $T < 90$ days) positively correlated with modelled soil moisture (Table S1). This suggests that catchment soil moisture plays a role for young water release in the HOAL catchment, which is further supported by the reasonably good simulation results of stable isotopes of water when only using soil moisture in the SAS function (NSE = 0.31). Therefore, the results correspond well to earlier research, where increasing catchment wetness resulted in younger water reaching the stream (Weiler and Naef, 2003; Zehe et al., 2006; Hrachowitz et al ., 2013; Remondi et al., 2018; Rodriguez et al., 2018; Sprenger et al., 2019).

Despite the selection of the SAS function based exclusively on catchment wetness being adequate for the HOAL catchment, the highly complex runoff generation mechanisms (Blöschl et al., 2016) with a quick runoff response particularly during

autumn and summer months, highlighted the need for an additional control on the SAS function shape (Fig. 5c, 7a). Indeed, the model performance was better (Fig. 5e) when including precipitation intensities in the SAS function (Fig. 4b). This indicates that the direct contribution of precipitation to streamflow during storm events with high precipitation intensities is important in the HOAL catchment. This behaviour can be explained by several factors that promote fast runoff that bypass resident water.

The incorporation of both soil moisture and precipitation intensity in the SAS function accounts for the non-linearity of flow processes, mimicking the behaviour not only of saturation-excess overland flow, but also that of infiltration-excess flow and other subsurface fast runoff flow processes that bypass flow with minimal interaction with resident water (e.g., tile drain flow). The non-linearity of flow processes in the HOAL catchment has been demonstrated through hydrometric analysis and visual observations, which have highlighted the potential controls of soil moisture and event precipitation on runoff (Blöschl et al., 2016; Exner-Kittridge et al., 2016; Vreugdenhil et al., 2022; Hovel et al., 2023; Szeles et al., 2024). Similarly, Vreugdenhil et al. (2022) showed that rainfall and soil moisture are significant and highly non-linear controls on overland flow and tile drainage flow in different parts of the HOAL. For instance, tile drainage in wetlands was more linearly related to soil moisture, whereas at the hillslope scale, it was more related to precipitation even at low-intensity rainfall. Therefore, it is plausible to assume that in the HOAL catchment, overland flow exhibits a threshold behaviour related to fast runoff generation occurring even at low-intensity rainfall.

Additionally, the HOAL catchment consists of a diverse range of soil types, with a high clay content between 20 % and 30 % (Blöschl et al., 2016). Different types of soils may introduce complexities due to surface and subsurface heterogeneity in soil hydraulic conductivity, which significantly influences the shapes of SAS functions (Danesh-Yazdi et al., 2018). As previously discussed by Danesh-Yazdi et al. (2018), subsurface heterogeneity in hydraulic conductivity imposes significant variation in the shape of the SAS function indeed, hydraulic conductivity in HOAL were found to be variable over two orders of magnitude, from as low as 1 mm h^{-1} to as high as 130 mm h^{-1}(Picciafuoco et al., 2019). Therefore, assuming a smooth functional form for the SAS function in heterogeneous systems may over-simplify its intrinsic variability concerning water age or age-ranked storage. This may also explain why incorporating soil moisture and precipitation intensity, as we did in Scenario 2, resulted in better model performance in the simulation of the $\delta^{18}O$ signal in streamflow.

Besides, the tile drainage system, which covers only 15 % of the catchment (Fig. 1), appeared to play an important role in fast flow generation. The close resemblance of the $\delta^{18}O$ signal in the tile drainage system with the precipitation $\delta^{18}O$ signal (Fig. 2e, 2f) provides evidence that some event precipitation contributes to the stream through the tile drain not only in winter but also in summer. A possible explanation for this process in summer months is that larger cracks in the clayey soils, which are directly connected to the tile drainage system, allow for preferential flow that is more dependent on precipitation intensity than on soil moisture. This corresponds with observations from Exner-Kittridge et al. (2016), who noted that in the HOAL catchment, macropore flow is observed in summer when the topsoil dries and forms cracks due to the high clay content. This emphasizes the critical role of soil texture and structure in influencing water movement during rainfall events.

4.2 Synthesis of streamflow generation processes in the HOAL catchment

The HOAL catchment exhibits a diverse and rapid hydrological response to precipitation events (Blöschl et al., 2016; Exner-Kittridge et al., 2016; Vreugdenhil et al., 2022). This is also evidenced by the on/off response of streamflow and the sharp transition between high-resolution event $\delta^{18}O$ signals and highly stable weekly $\delta^{18}O$ signals observed in the stream (Figure

2c, 2e, 2f). Tracer compositions measured at weekly intervals remained stable throughout the year (Fig. 2d). However, event-based samples and tile drainage samples showed similar $\delta^{18}O$ patterns to precipitation (Fig. 2f), indicating a sharp transition between fast flow processes and more stable groundwater flow. For several rain storms, the model reproduced the sharp fluctuations during events and a stable $\delta^{18}O$ signal between consecutive events (Fig. 5c) for both scenarios. Nevertheless, the model calibration based on Scenario 2 enhanced the model's sensitivity to the time scale of fast flow (Fig. 7a), further emphasizing the critical role of precipitation intensity in influencing hydrological responses in the catchment. In particular, infiltration-excess overland flow and precipitation-driven subsurface fast flow were identified as key flow processes, corroborating studies by Blöschl et al. (2016), Széles et al. (2020), and Silasari et al. (2017), who noted that both saturation-excess and infiltration-excess overland flow typically occur in valley bottoms during prolonged or intensive rainfall, with part of the event water entering the stream as overland flow. The hydrological behaviour of the HOAL catchment supports earlier findings by Kirchner et al. (2023), who noted that a rapid hydrological response often indicates rainwater quickly moving to channels via overland flow or fast subsurface pathways.

4.3 Catchment transit times

Transit time results indicated that event peaks were primarily a mixture of new precipitation water (T< 2 days) and water less than 7 days old that had been stored in the catchment. During events, the fraction of streamflow water for age $T < 7$ days, $7 < T < 90$ days, and $90 < T < 365$ days increased for both scenarios (Fig. 7a). However, on average, only ~ 4 % of the water was younger than 7 days, and ~7 % was younger than 90 days (Table 4). This aligns with the findings of previous studies elsewhere that have shown the majority of water contributing to streamflow as being old, a phenomenon that has been termed the "old water paradox" (Kirchner, 2003; McDonnell et al., 2010).

Nevertheless, the fraction of stream water younger than 7 days increased from 1 % to up to 45 % on an event scale depending on storm size (Fig. 8b, 9e). This indicated that most precipitation did not mobilise old water in the first place; instead, it drained directly into river networks and contributed to the stream via fast flow paths. This reflects results reported by Szeles et al. (2024), where their findings showed that the new water contribution averaged around 50 % during peak flows in selected large events in the HOAL catchment.

Given that the slope of the catchment is relatively low (8 %), another reason can be the high proportion of agriculturally used land, which tends to develop a compacted or sealed surface layer thus inhibiting or reducing infiltration during heavy rainfall events. Agricultural soils, particularly those with intensive tillage or limited vegetative cover are prone to surface sealing (Laloy and Bielders, 2010) during heavy rainfall events (e.g a reduction in infiltration capacity from heavy machinery, soil erosion processes). The impact of raindrops can break down soil aggregates at the surface, leading to the formation of a thin, compacted soil layer (i.e., a “soil crust”) that reduces infiltration capacity (Blöschl, 2022). This crust formation can be more pronounced in soils with higher silt content or weak aggregate stability, thereby favouring overland flow and quick runoff generation during heavy precipitation.

4.4 Catchment transit times variability with hydrological and hydroclimatic conditions

The fraction of stream water younger than 7 days, F_Q ($T < 7$ days), positively correlated with precipitation intensities (Fig. 8b), implying that the volume of event water transmitted to streamflow increases with storm size. Similar results were noted

by Szeles et al. (2024), who used hydrograph separation methods and highlighted that new water fractions during events increased with precipitation intensity in the HOAL catchment.

In contrast, the measured volumetric soil water content, *SWC* (%), did not strongly correlate with shorter transit times F_Q (T < 7 days) and F_Q (T < 90 days), for either scenario (Fig. 8c, 8f). This may seem contradictory, but it is plausible to assume that the effect of frequent fast flow in the HOAL catchment dominates and masks the underlying relationship between catchment wetness and transit times. Hövel et al. (2023) found that measured volumetric soil water content was weakly or not at all correlated with event runoff responses, reinforcing that precipitation intensity, rather than catchment wetness, can be the dominant driver of fast runoff generation.

Stream water fractions with transit times less than 90 days, F_Q (T < 90 days) were weakly correlated with discharge Q (mm d^{-1}) (r= 0.40 for S1 and 0.34 for S2), but were strongly positively correlated with precipitation intensity, P_I (mm d^{-1}) (r = 0.71 for S1 and 0.62 for S2) (Fig. 9d and 9e). These findings support the earlier study by Freyberg et al. (2018), who noted that low discharge sensitivity to high fractions of young water can indicate the dominance of fast runoff flow paths in the hydrological response. This behaviour persists regardless of the magnitude of precipitation events, particularly under conditions where the landscape promotes rapid water movement, such as in catchments with certain soil types or topographic features (such as the HOAL catchment). Such behaviour also points to well-developed subsurface flow paths (e.g., tile drains at the hillslope scale)) that directly transport water and solutes to the stream, highlighting the catchment's sensitivity to precipitation input.

4.5 Implications and limitations

Being conditional on the assumptions made throughout the modelling process, and notwithstanding potential uncertainties, high-frequency water-stable isotope data and model calibrations provide relatively strong evidence to support the key findings of this study: both soil moisture and precipitation intensity significantly influence hydrological responses and transit times in the HOAL catchment. This reflects non-linear flow behaviour and a shift towards younger water ages in the stream, particularly during autumn and summer. Soil-wetness-dependent and precipitation-intensity-conditional SAS functions may, therefore, be necessary to better capture and identify the mechanisms driving rapid streamflow generation and their associated timescales, notably in catchments where preferential flows and overland flow are dominant flow processes. The SAS functions based on both soil moisture and precipitation intensity resulted in an increased probability of rapid mobilization of young water which is critical for stream water quality and groundwater recharge.

Although the analysis is here limited to a small, agricultural catchment with flashy response, it is plausible to assume that the approach also is similarly valid in other settings with diverse hydrological characteristics and where rainfall intensity exceeds infiltration rates, leading to surface runoff or subsurface preferential pathways. By focusing on how soil moisture and precipitation intensity jointly influence younger water release, the insights of this study can help to develop water management strategies in, e.g., agricultural catchments. Managers could better schedule fertilizer applications to minimize nutrient leaching and reduce water quality deterioration.

There are some limitations in this study that need to be addressed and tested in future research. The model calibration based on both scenarios overestimated low flows during the summer of 2016, despite relatively higher precipitation during that year. This overestimation is likely linked to groundwater recharge processes being more complex than represented in the model structure. The overestimation of low flows began after an intense rainfall event (P > 50 mm d^{-1}, Fig. 2) followed by

several moderate-intensity events. A potential explanation is the activation of flow paths down to the depth of the tile drainage system or dominant subsurface lateral flow, which may have diverted water directly to the stream, bypassing groundwater infiltration and promoting interflow. Another possibility is the presence of a low-permeability unsaturated transition zone between the root zone and the groundwater table which may have delayed groundwater recharge. This could also explain why low flows in the winter and spring of 2017 were conversely underestimated. To fully evaluate these hypotheses and better estimate the recharge processes, additional field observations and more detailed studies focusing on subsurface dynamics and groundwater interactions are necessary.

Furthermore, the model calibration based on both scenarios showed limitations in simulating very low δ18O signals during the summer months, potentially due to the constant value assigned to the division parameter for infiltration-excess overland flows Cn (-). This parameter was kept constant in this study to maintain model simplicity. However, correlation results with hydrological and hydroclimatic drivers (Fig. 8) suggest that Cn (-) might also be a function of rainfall intensity and could increase with higher precipitation intensities. This indicates the need for a more dynamic representation of Cn to better capture its response to changing rainfall conditions.

Lastly, model calibration resulted in an infiltration-excess overland flow threshold precipitation intensity parameter Ptresh (mm d-1) range between 10–15 (mm d^{-1}) and 5–10 (mm d^{-1}) for Scenario 1 and Scenario 2, respectively (Fig. S1). While this may seem surprising at first, it can be reasonably explained by surface sealing during rainfall, which inhibits infiltration, particularly in areas affected by agricultural land use in the HOAL catchment in the summer, when the topsoil dries and cracks due to its high clay content. This parameter was also identified as a threshold for partitioning rainfall into preferential flow pathways and overland flow, thereby promoting fast runoff with minimal interaction with resident water to simulate $\delta^{18}O$ signals. Therefore, this threshold should not be considered a definitive marker for infiltration-excess overland flow. Instead, it can be a marker for any process that promotes rapid water movement in the HOAL catchment.

5 Conclusions

In this study, we showed that both soil moisture and precipitation intensity exert a significant influence on transit times In an agricultural catchment. The results also supported the hypothesis that the preferential release of younger water was controlled by soil moisture when precipitation intensity was below a threshold. However, when precipitation intensity exceeded a threshold, there was a higher probability of new water contributing to fast runoff with little exchange with stored water. The SAS functions based on both soil moisture and precipitation intensity resulted in an increased probability of rapid mobilization of young water FQ ($T < 7$ days), influenced by precipitation intensity particularly during autumn and summer months. Thus, in catchments where subsurface preferential flow and overland flow dominate, soil moisture-dependent and precipitation intensity-conditional SAS functions may be required to better constrain the age distribution of streamflow.

The findings also underscore the importance of the activation of fast flow paths in water quality variations within the catchment. Estimating young water contributions is essential not only for predicting how contaminants and nutrients are mobilized and transported during hydrological events but also for characterizing the underlying processes that govern the movement and mixing of water through the catchment. The results presented here focused on a small agricultural headwater catchment with substantial contributions from surface flow and shallow subsurface flow to streamflow. In other catchments with quick subsurface runoff and overland flow, accounting for precipitation intensity in transit times may also better reflect the hydrological dynamics and transport processes. For instance, by identifying periods or conditions under which

precipitation intensity triggers rapid flow through tile drains and preferential pathways, will allow watermanagers to develop guidance for better fertilizer application schedules to minimize nutrient export and reduce water quality deterioration. Similarly, insights into quick flow processes can guide the placement and timing of agricultural drainage systems to mitigate peak flows, inform stormwater management interventions (e.g., retention ponds or buffer strips) to reduce runoff peaks, and land-use practices to prevent or minimize the direct contribution.e runoff peaks, and land-use practices to prevent or minimize the direct contribution.

Code and data availability. An Python script that performs the calculations described in this paper will be deposited in an open-access Github archive repository and the link will be supplied with the final published paper.

Data availability. The data used in this study can be obtained from the Austrian Federal Agency for Water Management and upon request.

Author contributions. HT and MH jointly developed the model architecture for the catchment. HT performed the analysis presented here and drafted the paper. All authors discussed the design, contributed to the overall concept, and participated in the discussion and writing of the manuscript.

Competing interests. Some authors are members of the editorial board of the HESS journal.

Acknowledgments. We thank the Austrian Federal Agency for Water Management for providing the data Petzenkirchen catchment that we used in our analysis.This research is funded by the Austrian Science Fund (FWF–Österreichischer Wissenschaftsfonds) [grant number 10.55776/P34666]. The work of Hatice Turk was supported by the Doctoral School "Human River Systems in the 21st Century (HR21)" of the University of Natural Resources and Life Sciences, Vienna.

References

Abbott, B. W., Baranov, V., Mendoza-Lera, C., Nikolakopoulou, M., Harjung, A., Kolbe, T., et al. (2016). Using multi-tracer inference to move beyond single-catchment ecohydrology. Earth-Science Reviews, 160, 19–42. https://doi.org/10.1016/j.earscirev.2016.06.014

Angermann, L., Jackisch, C., Allroggen, N., Sprenger, M., Zehe, E., Tronicke, J., Weiler, M., & Blume, T. (2017). Form and function in hillslope hydrology: Characterization of subsurface flow based on response observations. Hydrology and Earth System Sciences, 21(8), 3727–3748. https://doi.org/10.5194/hess-21-3727-2017

Arthington, A. H., Kennen, J. G., Stein, E. D., & Webb, J. A. (2018). Recent advances in environmental flows science and water management—Innovation in the Anthropocene. Freshwater Biology, 63(8), 1022-1034. https://doi.org/10.1111/fwb.13108

Benettin, P., Bailey, S. W., Rinaldo, A., Likens, G. E., McGuire, K. J., & Botter, G. (2017). Young runoff fractions control streamwater age and solute concentration dynamics. Hydrological Processes, 31(14), 2982-2986. https://doi.org/10.1002/hyp.11243

Benettin, P., & Bertuzzo, E. (2018). Tran-SAS v1.0: A numerical model to compute catchment-scale hydrologic transport using StorAge Selection functions. Geoscientific Model Development, 11(4), 1627-1639. https://doi.org/10.5194/gmd-11-1627-2018

Benettin, P., Kirchner, J. W., Rinaldo, A., & Botter, G. (2015). Modeling chloride transport using travel time distributions at Plynlimon, Wales. Water Resources Research, 51(5), 3259-3276. https://doi.org/10.1002/2014WR016600

Benettin, P., Rodriguez, N. B., Sprenger, M., Kim, M., Klaus, J., Harman, C. J., van der Velde, Y., Hrachowitz, M., Botter, G., McGuire, K. J., Kirchner, J. W., Rinaldo, A., & McDonnell, J. J. (2022). Transit time estimation in catchments: Recent developments and future directions. Water Resources Research, 58(11). https://doi.org/10.1029/2022wr033096

Benettin, P., Soulsby, C., Birkel, C., Tetzlaff, D., Botter, G., & Rinaldo, A. (2017). Using SAS functions and high-resolution isotope data to unravel travel time distributions in headwater catchments. Water Resources Research, 53(3), 1864–1878. https://doi.org/10.1002/2016WR020117

Beven, K. J. (2006). A manifesto for the equifinality thesis. Journal of Hydrology, 320(1-2), 18–36. https://doi.org/10.1016/j.jhydrol.2005.07.007

Beven, K. J. (2010). Preferential flows and travel time distributions: Defining adequate hypothesis tests for hydrological process models. *Hydrological Processes, 24*(12), 1537–1547. https://doi.org/10.1002/hyp.7718

Beven, K. J., & Germann, P. (2013). Macropores and water flow in soils revisited. *Water Resources Research, 49*(6), 3071–3092. https://doi.org/10.1002/wrcr.20156

Blöschl, G., Blaschke, A. P., Broer, M., Bucher, C., Carr, G., Chen, X., Eder, A., Exner-Kittridge, M., Farnleitner, A., Flores-Orozco, A., Haas, P., Hogan, P., Kazemi Amiri, A., Oismüller, M., Parajka, J., Silasari, R., Stadler, P., Strauss, P., Vreugdenhil, M., & Zessner, M. (2016). The Hydrological Open Air Laboratory (HOAL) in Petzenkirchen: A hypothesis-driven observatory. *Hydrology and Earth System Sciences, 20*(1), 227–255. https://doi.org/10.5194/hess-20-227-2016

Blöschl, G.: Flood generation: process patterns from the raindrop to the ocean, Hydrol. Earth Syst. Sci., 26, 2469–2480, https://doi.org/10.5194/hess-26-2469-2022, 2022.

Botter, G., Bertuzzo, E., & Rinaldo, A. (2011). Catchment residence and travel time distributions: The master equation. Geophysical Research Letters, 38, 1-6. https://doi.org/10.1029/2011GL047666

Botter, G., Porporato, A., Rodriguez-Iturbe, I., & Rinaldo, A. (2009). Nonlinear storage-discharge relations and catchment streamflow regimes. Water Resources Research, 45(10). https://doi.org/10.1029/2008WR007658

Bower, L. M., Peoples, B. K., Eddy, M. C., & Scott, M. C. (2021). Quantifying flow–ecology relationships across flow regime class and ecoregions in South Carolina. Science of The Total Environment, 788, 149721. https://doi.org/10.1016/j.scitotenv.2021.149721

Bunn, S. E., & Arthington, A. H. (2002). Basic principles and ecological consequences of altered flow regimes for aquatic biodiversity. Environmental Management, 30(4), 492-507. https://doi.org/10.1007/s00267-002-2737-0

Criss, R. E., & Winston, W. E. (2008). Do Nash values have a value? Discussion and alternate proposals. Hydrological Processes, 22(14), 2723–2725. https://doi.org/10.1002/hyp.7072

Danesh-Yazdi, M., Klaus, J., Condon, L. E., & Maxwell, R. M. (2018). Bridging the gap between numerical solutions of travel time distributions and analytical storage selection functions. Hydrological Processes, 32(7), 1063–1076. https://doi.org/10.1002/hyp.11481

Eder, A., Exner-Kittridge, M., Strauss, P., & Blöschl, G. (2014). Re-suspension of bed sediment in a small stream – results from two flushing experiments. Hydrology and Earth System Sciences, 18(3), 1043–1052. https://doi.org/10.5194/hess-18-1043-2014

Exner-Kittridge, M., Strauss, P., Blöschl, G., Eder, A., Saracevic, E., & Zessner, M. (2016). The seasonal dynamics of the stream sources and input flow paths of water and nitrogen of an Austrian headwater agricultural catchment. Science of the Total Environment, 542, 935-945. https://doi.org/10.1016/j.scitotenv.2015.10.151

Fenicia, F., Wrede, S., Kavetski, D., Pfister, L., Hoffmann, L., Savenije, H. H. G., & McDonnell, J. J. (2010). Assessing the impact of mixing assumptions on the estimation of streamwater mean residence time. Hydrological Processes, 24(12), 1730–1741. https://doi.org/10.1002/hyp.7595

Fenicia, F., Savenije, H. H. G., Matgen, P., & Pfister, L. (2008). Understanding catchment behavior through stepwise model concept improvement. Water Resources Research, 44, W01402. https://doi.org/10.1029/2006WR005563

Freyberg, J. V., Allen, S. T., Seeger, S., Weiler, M., & Kirchner, J. W. (2018). Sensitivity of young water fractions to hydro-climatic forcing and landscape properties across 22 Swiss catchments. Hydrology and Earth System Sciences, 22(7), 3841–3861. https://doi.org/10.5194/hess-22-3841-2018

Freyberg, J. V., Rücker, A., Zappa, M., Schlumpf, A., Studer, B., & Kirchner, J. W. (2022). Four years of daily stable water isotope data in stream water and precipitation from three Swiss catchments. Scientific Data, 9(1), 1-10. https://doi.org/10.1038/s41597-022-01148-1

Fovet, O., Ruiz, L., Hrachowitz, M., Faucheux, M., & Gascuel-Odoux, C. (2015). Hydrological hysteresis and its value for assessing process consistency in catchment conceptual models. Hydrology and Earth System Sciences, 19(1), 105–123. https://doi.org/10.5194/hess-19-105-2015

Freyberg, J. V., Studer, B., Rinderer, M., & Kirchner, J. W. (2018). Studying catchment storm response using event- and pre-event-water volumes as fractions of precipitation rather than discharge. Hydrology and Earth System Sciences, 22(12), 5847–5865. https://doi.org/10.5194/hess-22-5847-2018

Gao, H., Hrachowitz, M., Schymanski, S. J., Fenicia, F., Sriwongsitanon, N., & Savenije, H. H. G. (2014). Climate controls how ecosystems size the root zone storage capacity at catchment scale. Geophysical Research Letters, 41(22), 7916–7923. https://doi.org/10.1002/2014GL061668

Girons Lopez, M., Vis, M. J. P., Jenicek, M., Griessinger, N., & Seibert, J. (2020). Assessing the degree of detail of temperature-based snow routines for runoff modelling in mountainous areas in central Europe. Hydrology and Earth System Sciences, 24(9), 4441–4461. https://doi.org/10.5194/hess-24-4441-2020

Goldsmith, G. R., Allen, S. T., Braun, S., Engbersen, N., González-Quijano, C. R., Kirchner, J. W., & Siegwolf, R. T. (2019). Spatial variation in throughfall, soil, and plant water isotopes in a temperate forest. Ecohydrology, 12(2), e2059. https://doi.org/10.1002/eco.2059

Gupta, H. V., Kling, H., Yilmaz, K. K., & Martinez, G. F. (2009). Decomposition of the mean squared error and NSE performance criteria: Implications for improving hydrological modelling. Journal of Hydrology, 377(1-2), 80–91. https://doi.org/10.1016/j.jhydrol.2009.08.003

Harman, C. (2019). Age-ranked storage-discharge relations: A unified description of spatially lumped flow and water age in hydrologic systems. Water Resources Research, 55(8), 7143–7165. https://doi.org/10.1029/2017WR022304

Harman, C. J. (2015). Time-variable transit time distributions and transport: Theory and application to storage-dependent transport of chloride in a watershed. Water Resources Research, 51(1), 1–30. https://doi.org/10.1002/2014WR015707

Horton, R. E. (1933). The role of infiltration in the hydrologic cycle. Eos, Transactions American Geophysical Union, 14(1), 446–460. https://doi.org/10.1029/TR014i001p00446

Hrachowitz, M., Benettin, P., Van Breukelen, B. M., Fovet, O., Howden, N. J. K., Ruiz, L., Van Der Velde, Y., & Wade, A. J. (2016). Transit times—The link between hydrology and water quality at the catchment scale. Wiley Interdisciplinary Reviews: Water, 3(5), 629-657. https://doi.org/10.1002/wat2.1155

Hrachowitz, M., Fovet, O., Ruiz, L., Euser, T., Gharari, S., Nijzink, R., Freer, J., Savenije, H. H. G., & Gascuel-Odoux, C. (2014). Process consistency in models: The importance of system signatures, expert knowledge, and process complexity. Water Resources Research, 50(9), 7445–7469. https://doi.org/10.1002/2014WR015484

Hrachowitz, M., Fovet, O., Ruiz, L., & Savenije, H. H. G. (2015). Transit time distributions, legacy contamination and variability in biogeochemical 1/f scaling: How are hydrological response dynamics linked to water quality at the catchment scale? Hydrological Processes, 29(24), 5241-5256. https://doi.org/10.1002/hyp.10546

Hrachowitz, M., Savenije, H. H. G., Bogaard, T. A., Tetzlaff, D., & Soulsby, C. (2013). What can flux tracking teach us about water age distribution patterns and their temporal dynamics? Hydrology and Earth System Sciences, 17(2), 533-564. https://doi.org/10.5194/hess-17-533-2013

Hrachowitz, M., Stockinger, M., Coenders-Gerrits, M., Van Der Ent, R. J., Bogena, H. R., Lücke, A., & Stumpp, C. (2021). Reduction of vegetation-accessible water storage capacity after deforestation affects catchment travel time distributions and

increases young water fractions in a headwater catchment. Hydrology and Earth System Sciences, 25(9), 4887–4915. https://doi.org/10.5194/hess-25-4887-2021

Hövel, A., Stumpp, C., Bogena, H., Lücke, A., Strauss, P., Blöschl, G., & Stockinger, M. (2024). Repeating patterns in runoff time series: A basis for exploring hydrologic similarity of precipitation and catchment wetness conditions. Journal of Hydrology, 629, 130585. https://doi.org/10.1016/j.jhydrol.2023.130585

Jothityangkoon, C., Sivapalan, M., & Farmer, D. L. (2001). Process controls of water balance variability in a large semi-arid catchment: Downward approach to hydrological model development. Journal of Hydrology, 254(1-4), 174–198. https://doi.org/10.1016/S0022-1694(01)00496-6

Kaandorp, V. P., de Louw, P. G. B., van der Velde, Y., & Broers, H. P. (2018). Transient groundwater travel time distributions and age-ranked storage-discharge relationships of three lowland catchments. Water Resources Research, 54(7), 4519–4536. https://doi.org/10.1029/2017WR022461

Kirchner, J. W. (2003). A double paradox in catchment hydrology and geochemistry. Hydrological Processes, 17(4), 871–874. https://doi.org/10.1002/hyp.5108

Kirchner, J. W., & Knapp, J. L. (2020). Calculation scripts for ensemble hydrograph separation. Hydrology and Earth System Sciences, 24(11), 5539–5558. https://doi.org/10.5194/hess-24-5539-2020

Kirchner, J. W., Feng, X., & Neal, C. (2000). Fractal stream chemistry and its implications for contaminant transport in catchments. Nature, 403(6769), 524–527. https://doi.org/10.1038/35000537

Kirchner, J. W. (2019). Quantifying new water fractions and transit time distributions using ensemble hydrograph separation: Theory and benchmark tests. Hydrology and Earth System Sciences, 23(1), 303-349. https://doi.org/10.5194/hess-23-303-2019

Kirchner, J. W., Benettin, P., & Van Meerveld, I. (2023). Instructive surprises in the hydrological functioning of landscapes. Annual Review of Earth and Planetary Sciences, 51, 303-329. https://doi.org/10.1146/annurev-earth-071822-100356

Klaus, J., & McDonnell, J. J. (2013). Hydrograph separation using stable isotopes: Review and evaluation. Journal of Hydrology, 505, 47–64. https://doi.org/10.1016/j.jhydrol.2013.09.006

Knighton, J., Kuppel, S., Smith, A., Soulsby, C., Sprenger, M., & Tetzlaff, D. (2020). Using isotopes to incorporate tree water storage and mixing dynamics into a distributed ecohydrologic modeling framework. Ecohydrology, 13(3), e2201. https://doi.org/10.1002/eco.2201

Knighton, J., Souter-Kline, V., Volkman, T., Troch, P. A., Kim, M., Harman, C., et al. (2019). Seasonal and topographic variations in ecohydrological separation within a small, temperate, snow-influenced catchment. Water Resources Research, 55(8), 6417–6435. https://doi.org/10.1029/2019WR025174

Kuppel, S., Tetzlaff, D., Maneta, M. P., & Soulsby, C. (2018). EcH2O-iso 1.0: Water isotopes and age tracking in a process-based, distributed ecohydrological model. Geoscientific Model Development, 11(8), 3045-3069. https://doi.org/10.5194/gmd-11-3045-2018

Kübert, A., Dubbert, M., Bamberger, I., Kühnhammer, K., Beyer, M., van Haren, J., Bailey, K., Hu, J., Meredith, L. K., Nemiah Ladd, S., & Werner, C. (2023). Tracing plant source water dynamics during drought by continuous transpiration measurements: An in-situ stable isotope approach. Plant, Cell & Environment, 46(1), 133–149. https://doi.org/10.1111/pce.14475

Laloy, E., & Bielders, C. L. (2010). Effect of intercropping period management on runoff and erosion in a maize cropping system. Journal of environmental quality, 39(3), 1001-1008. https://doi.org/10.2134/jeq2009.0239

Lutz, S. R., Krieg, R., Müller, C., Zink, M., Knöller, K., Samaniego, L., & Merz, R. (2018). Spatial patterns of water age: Using young water fractions to improve the characterization of transit times in contrasting catchments. Water Resources Research, 54(7), 4767-4784. https://doi.org/10.1029/2017WR022216

Loritz, R., Hassler, S. K., Jackisch, C., Allroggen, N., van Schaik, L., Wienhöfer, J., & Zehe, E. (2017). Picturing and modeling catchments by representative hillslopes. Hydrology and Earth System Sciences, 21(2), 1225–1249. https://doi.org/10.5194/hess-21-1225-2017

Maier, F., van Meerveld, I., & Weiler, M. (2021). Long-term changes in runoff generation mechanisms for two proglacial areas in the Swiss Alps II: Subsurface flow. Water Resources Research, 57, e2021WR030223. https://doi.org/10.1029/2021WR030223

McDonnell, J. J., & Beven, K. (2014). Debates The future of hydrological sciences: A (common) path forward? A call to action aimed at understanding velocities, celerities, and residence time distributions of the headwater hydrograph. Water Resources Research, 50, 5342–5350. https://doi.org/10.1002/2013WR015141

McDonnell, J. J., McGuire, K., Aggarwal, P., Beven, K. J., Biondi, D., Destouni, G., Dunn, S., James, A., Kirchner, J., Kraft, P., et al. (2010). How old is streamwater? Open questions in catchment transit time conceptualization, modeling, and analysis. Hydrological Processes, 24(12), 1745-1754. https://doi.org/10.1002/hyp.7796

McGuire, K. J., & McDonnell, J. J. (2006). A review and evaluation of catchment transit time modeling. Journal of Hydrology, 330(3-4), 543-563. https://doi.org/10.1016/j.jhydrol.2006.04.020

Nash, J. E., & Sutcliffe, J. V. (1970). River flow forecasting through conceptual models part I – A discussion of principles. Journal of Hydrology, 10(3), 282–290. https://doi.org/10.1016/0022-1694(70)90255-6

Nijzink, R., Hutton, C., Pechlivanidis, I., Capell, R., Arheimer, B., Freer, J., Han, D., Wagener, T., McGuire, K., Savenije, H., & Hrachowitz, M. (2016). The evolution of root-zone moisture capacities after deforestation: A step towards hydrological predictions under change? Hydrology and Earth System Sciences, 20(11), 4775–4799. https://doi.org/10.5194/hess-20-4775-2016

Nico Hachgenei, Guillaume Nord, Lorenzo Spadini, Patrick Ginot, Céline Voiron, et al.. Transit timetracing using wetness-adaptive StorAge Selection functions-application to a Mediterranean catchment.Journal of Hydrology, 2024, 638, ff10.1016/j.jhydrol.2024.131267

Pavlin, L., Széles, B., Strauss, P., Blaschke, A. P., & Blöschl, G. (2021). Event and seasonal hydrologic connectivity patterns in an agricultural headwater catchment. Hydrology and Earth System Sciences, 25(4), 2327-2352. https://doi.org/10.5194/hess-25-2327-2021

Picciafuoco, T., Morbidelli, R., Flammini, A., Saltalippi, C., Corradini, C., Strauss, P., & Blöschl, G. (2019). On the estimation of spatially representative plot scale saturated hydraulic conductivity in an agricultural setting. Journal of hydrology, 570, 106-117.https://doi.org/10.1016/j.jhydrol.2018.12.044

Remondi, F., Botter, M., Burlando, P., & Fatichi, S. (2019). Variability of transit time distributions with climate and topography: A modeling approach. Journal of Hydrology, 569, 37-50. https://doi.org/10.1016/j.jhydrol.2018.11.011

Remondi, F., Kirchner, J. W., Burlando, P., & Fatichi, S. (2018). Water flux tracking with a distributed hydrological model to quantify controls on the spatio-temporal variability of transit time distributions. Water Resources Research, 54(5), 3081-3099. https://doi.org/10.1002/2017WR021689

Rinaldo, A., Benettin, P., Harman, C. J., Hrachowitz, M., McGuire, K. J., Van Der Velde, Y., Bertuzzo, E., & Botter, G. (2015). Storage selection functions: A coherent framework for quantifying how catchments store and release water and solutes. Water Resources Research, 51(6), 4840-4847. https://doi.org/10.1002/2015WR017273

Rinaldo, A., Beven, K. J., Bertuzzo, E., Nicotina, L., Davies, J., Fiori, A., Russo, D., & Botter, G. (2011). Catchment travel time distributions and water flow in soils. Water Resources Research, 47, W07537. https://doi.org/10.1029/2011WR010478

Rodriguez, N. B., & Klaus, J. (2019). Catchment travel times from composite StorAge Selection functions representing the superposition of streamflow generation processes. Water Resources Research, 55(12), 9292–9314. https://doi.org/10.1029/2019WR024973

Rodriguez, N. B., McGuire, K. J., & Klaus, J. (2018). Time-varying storage-water age relationships in a catchment with a Mediterranean climate. Water Resources Research, 54(6), 3988-4008. https://doi.org/10.1029/2017WR021964

Silasari, R., Parajka, J., Ressl, C., Strauss, P., & Blöschl, G. (2017). Potential of time-lapse photography for identifying saturation area dynamics on agricultural hillslopes. Hydrological Processes, 31(19), 3610–3627. https://doi.org/10.1002/hyp.11272

Sprenger, M., Stumpp, C., Weiler, M., Aeschbach, W., Allen, S. T., et al. (2019). The demographics of water: A review of water ages in the critical zone. Reviews of Geophysics, 57(3), 800–834. https://doi.org/10.1029/2018RG000633

Storn, R., & Price, K. (1997). Differential evolution – A simple and efficient heuristic for global optimization over continuous spaces. Journal of Global Optimization, 11(4), 341–359. https://doi.org/10.1023/A:1008202821328

Széles, B., Parajka, J., Hogan, P., Silasari, R., Pavlin, L., Strauss, P., & Blöschl, G. (2020). The added value of different data types for calibrating and testing a hydrologic model in a small catchment. Water Resources Research, 56(1). https://doi.org/10.1029/2019WR026153

Széles, B., Holko, L., Parajka, J., Stumpp, C., Stockinger, M., Komma, J., Rab, G., Wyhlidal, S., Schott, K., Hogan, P., Pavlin, L., Strauss, P., Schmaltz, E., & Blöschl, G. (2024). Comparison of two isotopic hydrograph separation methods in the Hydrological Open Air Laboratory, Austria. Hydrological Processes, 38(7). https://doi.org/10.1002/hyp.15222

Tiefenbacher, A., Weigelhofer, G., Klik, A., Mabit, L., Santner, J., Wenzel, W., & Strauss, P. (2021). Antecedent soil moisture and rain intensity control pathways and quality of organic carbon exports from arable land. Catena, 202, 105297. https://doi.org/10.1016/j.catena.2021.105297

van der Velde, Y., Heidbüchel, I., Lyon, S., Nyberg, L., Rodhe, A., Bishop, K., & Troch, P. (2015). Consequences of mixing assumptions for time-variable travel time distributions. Hydrological Processes, 29(15), 3460–3474. https://doi.org/10.1002/hyp.10372

van der Velde, Y., Torfs, P. J. J. F., van der Zee, S. E. A. T. M., & Uijlenhoet, R. (2012). Quantifying catchment-scale mixing and its effect on time-varying travel time distributions. Water Resources Research, 48(6). https://doi.org/10.1029/2011WR011310

Vreugdenhil, M., Széles, B., Wagner, W., Strauss, P., Oismüller, M., Parajka, J., Blöschl, G., & Hogan, P. (2022). Non-linearity in event runoff generation in a small agricultural catchment. Hydrological Processes, 36(5), e14667. https://doi.org/10.1002/hyp.14667

Wang, S., Hrachowitz, M., Schoups, G., & Stumpp, C. (2023). Stable water isotopes and tritium tracers tell the same tale: no evidence for underestimation of catchment transit times inferred by stable isotopes in StorAge Selection (SAS)-function models. Hydrology and Earth System Sciences, 27(16), 3083-3114. https://doi.org/10.5194/hess-27-3083-2023

Wang, S., Hrachowitz, M., & Schoups, G. (2024). Multi-decadal fluctuations in root zone storage capacity through vegetation adaptation to hydro-climatic variability have minor effects on the hydrological response in the Neckar River basin, Germany. Hydrology and Earth System Sciences, 28(17), 4011-4033. https://doi.org/10.5194/hess-28-4011-2024

Wang, S., Hrachowitz, M., Schoups, G., & Störiko, A. (2025). Multi-decadal stability of water ages and tracer transport in a temperate-humid river basin. Environmental Research Letters, 20(2), 024046 . DOI 10.1088/1748-9326/ada8c1

Weiler, M., & McDonnell, J. J. (2007). Conceptualizing lateral preferential flow and flow networks and simulating the effects on gauged and ungauged hillslopes. Water Resources Research, 43(3), W03403. https://doi.org/10.1029/2006WR004867

Weiler, M., McGlynn, B. L., McGuire, K. J., & McDonnell, J. J. (2003). How does rainfall become runoff? A combined tracer and runoff transfer function approach. Water Resources Research, 39(11). https://doi.org/10.1029/2003WR002331

Yadav, M., Wagener, T., & Gupta, H. V. (2007). Regionalization of constraints on expected watershed response behavior for improved predictions in ungauged basins. Advances in Water Resources, 30(8), 1756–1774. https://doi.org/10.1016/j.advwatres.2007.01.005

Zehe, E., Lee, H., & Sivapalan, M. (2006). Dynamical process upscaling for deriving catchment scale state variables and constitutive relations for meso-scale process models. Hydrology and Earth System Sciences, 10(6), 981–996. https://doi.org/10.5194/hess-10-981-2006

Zuber, A. (1986). On the interpretation of tracer data in variable flow systems. Journal of Hydrology, 86(1-2), 45–57. https://doi.org/10.1016/0022-1694(86)90005-3